1

A Mixed Convection Study in Inclined Channels with Discrete Heat Sources

Paulo M. Guimarães and Genésio J. Menon
Federal University of Itajubá
Brazil

1. Introduction

In the last two decades, heat transfer study on discrete heat sources has become a subject of increased interest due to advances in the electronics industry. Increased power dissipation is the most significant feature of new generation electronic devices and more significant heat flux densities are obtained as a result of miniaturization. Consequently, the assumption of cooling of electronic devices has increased interest in the analysis of fluid flow and heat transfer in discrete heating situations. Previous works have studied the natural, mixed, and forced convection in inclined channels due to their practical applications such as electronic systems, high performance heat exchangers, chemical process equipments, combustion chambers, environmental control systems and so on.

An interesting study was reported on the fluid flow and heat transfer characteristics associated with cooling an in-line array of discrete protruding heated blocks in a channel by using a single laminar slot air jet (Arquis et al., 2007). Numerical experiments were carried out for different values of jet Reynolds number, channel height, slot width, spacing between blocks, block height, and block thermal conductivity. The effects of variation of these parameters were detailed to illustrate important fundamental and practical results that are relevant to the thermal management of electronic packages. In general, the effective cooling of blocks was observed to increase with the increase of Reynolds number and the decrease of channel height. Circulation cells that may appear on the top surface of the downstream blocks were shown to decrease the value of Nusselt number for these blocks. The values of surface averaged Nusselt number attained their maximum at the block just underneath the impinging air jet, decreased for the downstream blocks, and approximately reached a constant value after the third block.

A numerical study (Madhusudhana & Narasimham, 2007) was carried out on conjugate mixed convection arising from protruding heat generating ribs attached to substrates forming a series of vertical parallel plate channels. A channel with periodic boundary conditions in the transverse direction was considered for analysis where identical disposition and heat generation of the ribs on each board were assumed. The governing equations were discretised using a control volume approach on a staggered mesh and a pressure correction method was employed for the pressure–velocity coupling. The solid regions were considered as fluid regions with infinite viscosity; and the thermal coupling between the solid and fluid regions was taken into account by the harmonic thermal

conductivity method. Parametric studies were performed by varying the heat generation based on Grashof number in the range 10^4–10^7 and the fan velocity was based on Reynolds number in the range 0–1500, with air as the working fluid. In pure natural convection, the induced mass flow rate varied at 0.44 power of Grashof number. The heat transferred to the working fluid via substrate heat conduction was found to account for 41–47% of the heat removal from the ribs.

The optimum position of a discrete heater was determined by maximizing the conductance and the heat transfer and volume flow rate with the discrete heater at its optimum position in open cavities by using the finite difference-control volume numerical method and considering air (Muftuoglu & Bilgen, 2007). The relevant governing parameters were: the Rayleigh numbers from 10^6 to 10^{12}, the cavity aspect ratio from 0.5 to 2, the wall thickness from 0.05 to 0.15, the heater size from 0.15 to 0.6, and the conductivity ratio from 1 to 50. They found that the global conductance was an increasing function of the Rayleigh number and the conductivity ratio, and a decreasing function of the wall thickness. The best thermal performance was achieved by positioning the discrete heater eccentrically and slightly closer to the bottom. The Nusselt number and the volume flow rate in and out the open cavity were an increasing function of the Rayleigh number and the wall thickness, and a decreasing function of the conductivity ratio. The Nusselt number was a decreasing function of the cavity aspect ratio and the volume flow rate was an increasing function of it.

Another work conducted a numerical investigation of conjugate convection with surface radiation from horizontal channels with protruding heat sources (Premachandran & Balaji, 2006). The air flow was assumed to be steady, laminar, incompressible, and hydrodynamically and thermally developed. The geometric parameters such as spacing between the channel walls, size of the protruding heat sources, thickness of the substrate and the spacing between the heat sources were fixed. One of the most relevant conclusions was that while carrying out a thermal analysis of a stack of circuit boards with electronic chips (discrete heat sources), the consideration of radiation heat transfer was absolutely essential to accurately predict the non-dimensional maximum temperature.

The mixed convection heat transfer in a top-and-bottom-heated rectangular channel with discrete heat sources using air was experimentally investigated (Dogan et al., 2005). The lower and upper surfaces of the channel were equipped with 8x4 flush-mounted heat sources subjected to uniform heat flux. The lateral and remaining lower and upper walls were insulated. The experimental study was carried out for an aspect ratio equal to 6, Reynolds numbers varying from 955 to 2220 and modified Grashof numbers $Gr^*=1.7\times10^7$ to 6.7×10^7. The surface temperature and Nusselt number distributions on the discrete heat sources were obtained. Results showed that the surface temperatures increased with increasing Grashof number. The row-averaged Nusselt numbers decreased with the row number and then, they showed an increase towards the exit as a result of heat transfer enhancement due to the invigoration of buoyancy forces that affected the secondary flow.

A work investigated melting from heat sources that are flush-mounted on discretely heated rectangular vertical enclosures (Binet & Lacroix, 2000). It finds its application in design and operation of thermal energy storage units and the cooling of electronic equipment. The results showed that there were benefits of discrete heating when it comes to optimizing the melting process. The aspect ratio was an important factor that may have led to controlled temperatures on the heat modules. For aspect ratios over 4, controlled temperatures and long melting time were obtained. On the other hand, for aspect ratios up to 4, the source

span influence was important, whenever it was less than 0.45, and eventually, the melting times were shorter and the temperatures on the sources remained equal and moderate throughout the melting process.

The turbulent convection heat transfer was experimentally investigated in an array of discrete heat sources inside a rectangular channel filled with air (Baskaya et al., 2005). The lower surface of the channel was equipped with 8x4 flush-mounted heat sources subjected to uniform heat flux. The sidewalls and the upper wall were insulated. The experimental parametric study was made for a constant aspect ratio, different Reynolds numbers, and modified Grashof numbers. Results showed that surface temperatures increased with increasing Grashof number and decreased with increasing Reynolds number. However, the increase in the buoyancy forces affected the secondary flow and the onset of instability, and, hence, the temperatures levelled off and even dropped as a result of heat transfer enhancement. This outcome could also be observed from the variation of the row-averaged Nusselt number showing an increase towards the exit.

A constructal theory was applied to the fundamental problem of how to arrange discrete heat sources on a wall cooled by forced convection (Silva et al., 2004). They aimed to maximize the conductance between the discrete heated wall and the fluid, that is, to minimize the temperature of the hot spot on the wall, when the heat generation rate was specified. The global objective was achieved by the generation of flow configuration, in this case, the distribution of discrete heat sources. Two different analytical approaches were used: (i) large number of small heat sources, and (ii) small number of heat sources with finite length, which were mounted on a flat wall. Both analyses showed that the heat sources should have been placed non-uniformly on the wall, with the smallest distance between them near the tip of the boundary layer. When the Reynolds number was high enough, then, the heat sources should have been mounted flushed against each other, near the entrance of the channel. The analytical results were validated by a numerical study of discrete heat sources that were non-uniformly distributed inside a channel formed by parallel plates.

In the present chapter, a heat transfer study in an inclined rectangular channel with heat sources is conducted. The heat source vertical and horizontal positions are also considered. Emphasis is given to the heat transfer distributions on the heat modules, showing their correlation with velocities due to their importance when thermal control in electronic equipments is aimed.

2. Problem description

Figure (1) depicts three heat source lay-outs that will be studied. A mixed convection study is performed in a channel with height H, length L, and inclination γ. At the inlet, a constant velocity and temperature profiles, U_o and T_o, respectively, are imposed. The open boundary conditions (OBC) are arranged in a way that they are calculated, that is, the pressure terms are retrieved in the calculation (Heinrich & Pepper, 1999). Therefore, nothing is directly applied at the open boundary. For more information on this, the reader should refer to (Heinrich & Pepper, 1999). The reference and cooling temperatures T_o and T_c, respectively, are the same and equal to zero. Initially, the internal fluid domain has velocities and temperatures equal to zero. All surfaces present the no-slip condition. The regime is non-steady, two-dimensional, and laminar. Next, all three situations are described.

One heat source: One heat source with heat flux q′ of finite length B is placed at x_1 on the lower surface. Heat transfer will be analyzed according to the variation of the Reynolds

number (Re), the Grashof number (Gr), and the inclination angle (γ). B = H, and L = 15H. *Two heat sources*: Two constant-flux heat sources, $q'_1$and q'_2 of finite length B are placed at x_1 and x_2 on the lower surface. The distance between the heaters is d. Throughout this case, the geometry has x_1 = 5H, x_2 = 7H, 8H, and 9H, and hence characterizing d = 1, 2, and 3, respectively. Heat transfer will be analyzed according to the variation of Re, Gr, and d. The inclination angle is zero, that is, the channel is in the horizontal position. B = H, and L = 15H. *Three heat sources*: It is an inclined rectangular channel with height H and length L. Three constant heat sources q'_1, q'_2, and q'_3 of length B are placed on the bottom wall at x_1, x_2, and x_3, respectively. The remaining lower wall is isolated. The upper wall in contact with the fluid is constantly cooled at a uniform temperature T_c. At the inlet, constant velocity and temperature profiles, U_o and T_o, are applied as boundary conditions. Throughout this case, the geometry has x_1 = 6.75H, x_2 = 14.50H, x_3 = 22.25H, B = H = 1, and L = 30H.

3. Problem formulation and the numerical method

The problem governing equation set is given by the continuity, Navier-Stokes, and energy equations. Variables u and v are, respectively, the velocity components in x and y directions, T is the fluid temperature, t′ is the dimensional time, q′ is the heat flux, D_T is the fluid thermal diffusivity, β_T is the thermal expansion coefficient, ν is the kinematics viscosity, g is the gravity acceleration, and ρ_0 is the fluid density and $T_o = T_c$ and $\Delta T = T_h - T_c$. Considering the Boussinesq approximation and the following dimensionless parameters:

$$X=\frac{x}{B};\ Y=\frac{y}{B};\ U=\frac{u}{U_o};\ V=\frac{v}{U_o};\ P=\frac{p}{\rho_0 U_o^{\,2}};\ t=\frac{t'}{(B/U_o)'};\ \theta=(T-T_o)/(q'B/D_T)$$
$$Fr=\frac{\mathrm{Re}^2}{Gr}=\frac{U_o^{\,2}}{\beta_T g\Delta TB};\ \ \mathrm{Pr}=\frac{\nu}{D_T};\ Gr=\frac{\beta_T g\Delta TB^3}{\nu^2};\ \ \mathrm{Re}=\frac{U_o\rho_0 B}{\mu};\tag{1}$$

where Fr, Pr, Gr, Re, U_o, and μ are, respectively, the Froude number, the Prandtl number, the Grashof number, the Reynolds number, the average velocity, and the dynamic viscosity, the dimensionless governing equations can be cast into the following form:

$$\frac{\partial U}{\partial X}+\frac{\partial V}{\partial Y}=0;\tag{2}$$

$$\frac{\partial U}{\partial t}+U\frac{\partial U}{\partial X}+V\frac{\partial U}{\partial Y}=-\frac{\partial P}{\partial X}+\frac{1}{\mathrm{Re}}\left(\frac{\partial^2 U}{\partial X^2}+\frac{\partial^2 U}{\partial Y^2}\right)+\sin(\gamma)\frac{\theta}{Fr};\tag{3}$$

$$\frac{\partial V}{\partial t}+U\frac{\partial V}{\partial X}+V\frac{\partial V}{\partial Y}=-\frac{\partial P}{\partial Y}+\frac{1}{\mathrm{Re}}\left(\frac{\partial^2 V}{\partial X^2}+\frac{\partial^2 V}{\partial Y^2}\right)+\cos(\gamma)\frac{\theta}{Fr};\tag{4}$$

$$\frac{\partial \theta}{\partial t}+U\frac{\partial \theta}{\partial X}+V\frac{\partial \theta}{\partial Y}=\frac{1}{\mathrm{Re}\,\mathrm{Pr}}\left(\frac{\partial^2 \theta}{\partial X^2}+\frac{\partial^2 \theta}{\partial Y^2}\right);\tag{5}$$

The dimensionless boundary conditions are:

$U = V = 0$ (all walls); $\theta = 0$ (inlet and upper walls); $U = 1$ (inlet) and $\frac{\partial\theta}{\partial Y} = -1$ (heat sources).

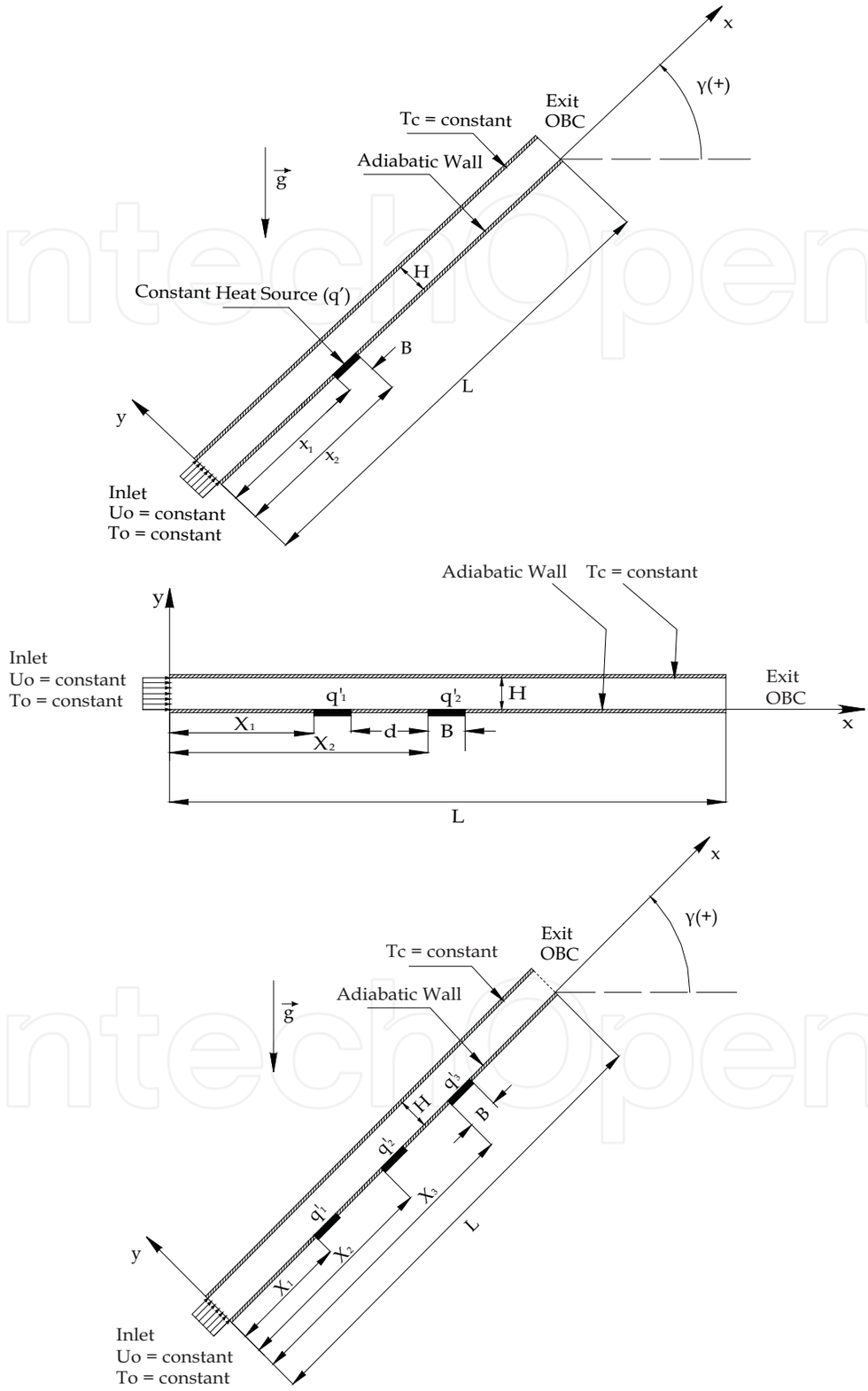

Fig. 1. Geometries and boundary conditions: cases with one, two, and three heat sources

Applying the Petrov-Galerkin formulation and the Penalty technique to Eqs. (2) to (5), the weak forms of the conservation equations may be written as follows:

$$\int_\Omega N_i\left[\frac{\partial U}{\partial t}+\frac{1}{\mathrm{Re}}\left(\frac{\partial N_i}{\partial X}\frac{\partial U}{\partial X}+\frac{\partial N_i}{\partial Y}\frac{\partial U}{\partial Y}\right)\right]d\Omega+\int_\Omega^R \lambda\frac{\partial N_i}{\partial X}\left(\frac{\partial U}{\partial X}+\frac{\partial V}{\partial Y}\right)d\Omega= \int_\Omega\left[\left(N_i+P_{i1}\right)\left(U\frac{\partial U}{\partial X}+V\frac{\partial U}{\partial Y}\right)+N_i\sin(\gamma)\frac{\theta}{Fr}\right]d\Omega-\int_{\Gamma_0}N_i\,p\,n_x\,d\Gamma \tag{6}$$

$$\int_\Omega N_i\left[\frac{\partial V}{\partial t}+\frac{1}{\mathrm{Re}}\left(\frac{\partial N_i}{\partial X}\frac{\partial V}{\partial X}+\frac{\partial N_i}{\partial Y}\frac{\partial V}{\partial Y}\right)\right]d\Omega+\int_\Omega^R \lambda\frac{\partial N_i}{\partial Y}\left(\frac{\partial U}{\partial X}+\frac{\partial V}{\partial Y}\right)d\Omega= \int_\Omega\left[\left(N_i+P_{i1}\right)\left(U\frac{\partial V}{\partial X}+V\frac{\partial V}{\partial Y}\right)+N_i\cos(\gamma)\frac{\theta}{Fr}\right]d\Omega-\int_{\Gamma_0}N_i\,p\,n_y\,d\Gamma \tag{7}$$

$$\int_\Omega\left[N_i\frac{\partial\theta}{\partial t}+\frac{1}{\mathrm{Re}\,\mathrm{Pr}}\left(\frac{\partial N_i}{\partial X}\frac{\partial\theta}{\partial X}+\frac{\partial N_i}{\partial Y}\frac{\partial\theta}{\partial Y}\right)\right]d\Omega=\int_\Omega\left(N_i+P_{i2}\right)\left(U\frac{\partial\theta}{\partial X}+V\frac{\partial\theta}{\partial Y}\right)d\Omega+\int_{\Gamma_1}N_i\,q\,d\Gamma \tag{8}$$

where the dependent variables are approximated through the finite element method by:

$$\Phi(X,Y,t)=\sum_j N_j(X,Y)\Phi_j(t);\;\; p(X,Y,t)=\sum_k M_k(X,Y)p_k(t) \tag{9}$$

Ni and Nj are linear shape functions for the quantity Φ, that is, for U, V, and θ. M_k are the pressure piecewise element shape functions. The Petrov-Galerkin perturbations P_{ij}, which are only applied to the convective terms, are defined as:

$$P_{ij}=k_j\left(U\frac{\partial N_i}{\partial X}+V\frac{\partial N_i}{\partial Y}\right);\;\; k_j=\frac{\alpha_j\bar{h}}{|V|};\;\; \alpha_j=\coth\frac{\gamma_j}{2}-\frac{2}{\gamma_j};\;\; \gamma_j=\frac{|V|\bar{h}}{\varepsilon_j};\;\; j=1,2 \tag{10}$$

where γ is the element Péclet number, $|V|$ is the absolute value of the velocity vector that represents the fluid average velocity within the element, $\bar{h}$ is the element average size, $\varepsilon_1=1/\mathrm{Re}$, $\varepsilon_2=1/Pe$, and λ is the Penalty parameter equal to 10^9. Fig. (2) shows the general linear quadrilateral element with $|V|$ and $\bar{h}$.

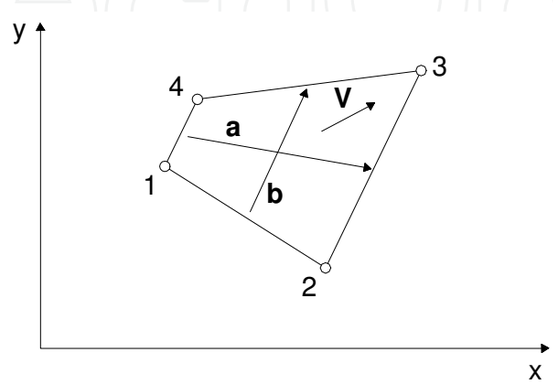

Fig. 2. General bilinear quadrilateral element with vectors a and b and element velocity V

The element average size $\bar{h}$ in the flow direction is given by :

$$\bar{h} = \frac{1}{|\mathbf{V}|}\left(|h_1| + |h_2|\right) \tag{11}$$

where h_1, h_2, a, and b are defined as:

$$h_1 = \mathbf{a.V}\ ;\ h_2 = \mathbf{b.V} \tag{12}$$

$$a_1 = \frac{1}{2}\left(x_2 + x_3 - x_1 - x_4\right);\ a_2 = \frac{1}{2}\left(y_2 + y_3 - y_1 - y_4\right);$$
$$b_1 = \frac{1}{2}\left(x_3 + x_4 - x_1 - x_2\right);\ b_2 = \frac{1}{2}\left(y_3 + y_4 - y_1 - y_2\right) \tag{13}$$

Vectors **a** and **b** are the vectors that are limited by the middle points of opposite sides and h_1 and h_2 are the projections of these vectors on the flow direction. The most important characteristic of the Petrov-Galerkin method is that it does not add any transversal diffusion to the flow, that is, an orthogonal diffusion to the flow direction. α_j is the so-called artificial diffusion or the equilibrium diffusion added to the convective terms. In fact, it is the optimum diffusion found between the diffusions provided by the traditional Galerkin method and the upwind one, which are respectively, under-diffused and over-diffused methods. This helps one solve some numerical oscillations which arise from the 'battle' between elliptic and hyperbolic problems. λ is a problem-independent value, given that the governing parameters do not change drastically (Bercovier & Engelman, 1979; Carey & Krishnan, 1982). This parameter must have a high value in order to have a 'quasi-incompressible' problem. Indeed, the Penalty theory comes from the Stokes viscosity law. Recalling the pressure formula:

$$p = p_s - \left(\bar{\mu} + \frac{2}{3}\mu\right)\nabla.\mathbf{V} \tag{14}$$

where p_s is the static or thermodynamic component of pressure, p is the average pressure, $\bar{\mu}$ is the second viscosity coefficient, and μ is the first viscosity.

Stokes hypothesized that $p = p_s$, hence, $\bar{\mu} = -\frac{2}{3}\mu$. It was shown to be true for some gases; however experiments revealed that with liquids, $\lambda = \left(\bar{\mu} + \frac{2}{3}\mu\right)$ is a positive quantity that is much larger than μ. λ represents the fluid bulk viscosity. If the fluid is perfectly incompressible, λ tends to be infinite. The basic idea of the Penalty formulation is to express the pressure by

$$P = p - p_s = -\lambda\nabla.\mathbf{V}\ ; \tag{15}$$

where λ is a very large number, and P is a modified pressure, which can be seen in Eqs. (3) and (4). For linear interpolation of velocities, the pressure inside the element can be expressed by:

$$P^e = -\frac{\lambda}{A^e}\int_e^R \left(\frac{\partial U}{\partial X} + \frac{\partial V}{\partial Y}\right) de \tag{16}$$

where e denotes the element restriction and Ae the element area.
Let one neglect some terms in the momentum equations and attain to those in the stiffness matrix, just to facilitate understanding of the Penalty parameter study. Substituting Eq. (16) in (3) and (4) with some manipulation and neglection of some terms which are now not important, the final linear system of equations would present this expression.

$$\left[\mu \mathbf{K}_1 + \lambda \mathbf{K}_2\right]\mathbf{d} = \mathbf{F} \tag{17}$$

where $\mathbf{F}$ is the force matrix generated by the boundary conditions, $\mathbf{d}$ is the velocity vector only. Now, let one suppose that $\mathbf{K}_2$ is not singular and λ is increased more and more in an attempt to reach incompressibility. Because μ and $\mathbf{K}_1$ are constant as λ is increased, they can be neglected and the solution to Eq. (17) would be:

$$\mathbf{d} = \frac{1}{\lambda}\mathbf{K}_2^{-1}\mathbf{F} \tag{18}$$

Being that $\mathbf{K}_2$ and $\mathbf{F}$ are also constant, it can be noted that $\mathbf{d} \to 0$ as $\lambda \to \infty$. This is called 'locking' and is strictly related to the incompatibility between the pressure and velocity spaces. Hence, the only solution to this space is the velocity vector $\mathbf{V} = 0$. It must be guaranteed that the Penalty matrix $\mathbf{K}_2$ be singular. This is accomplished by using the selective reduced integration of the Penalty term and the least square quadrature with a degree of precision lower than the necessary to guarantee an optimum convergence rate of matrix $\mathbf{K}_1$. Therefore, Fig. (3) shows a pair of elements used here in order to avoid locking.

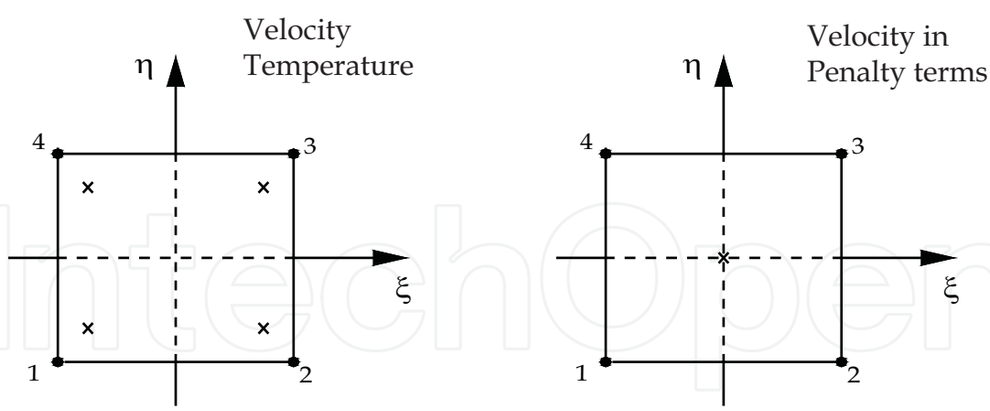

Fig. 3. Real (a) and parent (b) elements for full and reduced integration, respectively

The time integration is accomplished by the Euler backward semi-implicit method. Moreover, the convective and viscous terms are, respectively, calculated explicitly and implicitly. Finally, the average Nusselt number along a surface S of a heat source can be written as follows:

$$Nu = \frac{1}{S}\int_S \left[\frac{1}{\theta}\right] ds \tag{19}$$

4. Validation and mesh independency

The algorithm is validated by comparing the results of the present work with both the ones obtained in experimental and numerical investigations. The first comparison is accomplished not only by using experimental results (Lee & Mateescu, 1998; Armaly et al., 1983), but also by numerical ones (Lee & Mateescu, 1998; Gartling, 1990; Kim & Moin, 1985, and Sohn, 1988). The air flow of the present comparison analysis is taken as two-dimensional, laminar, incompressible, and under the unsteady regime. The domain is a horizontal upstream backward-facing step channel whose inlet has a fully developed velocity profile given by u = 24 y (0.5-y) $\overline{U}$ and v = 0 in which Re = 800. A structured mesh with 6000 quadrilateral linear elements with ΔX = 0.10 e ΔY = 0.05 and time step of Δt = 0.05 are used. By comparing the flow separation distance on the upper surface, its reattachment distance on the bottom surface and its reattachment distance on the upper wall, the deviations are in the range from 0.8% to 17.85%. Out of the 14 calculated deviations, just two are over 10%. Therefore, the results of the first comparison agree well with the ones from the literature. The second comparison is performed with the numerical results (Comini et al., 1997). The contrasting study is carried out by considering a problem involving mixed convective heat transfer with the flow being two-dimensional, laminar, and incompressible in the unsteady regime. This is a benchmark problem which involves the Rayleigh-Bérnard convection in a rectangular channel. In this case, some values are chosen such as Re = 10, Pr = 0.67, and Fr = 1/150. The grid has 4000 quadrilateral linear elements with $\Delta x = 0.1$, $\Delta y = 0.15$, $\Delta t = 0.01$ and 1000 iterations. After approximately iteration 500, the regime turns to be quasi-periodic with the average Nusselt number on the upper wall oscillating around a mean value of 2.44. This value agrees satisfactorily with 2.34 (Comini et al., 1997), resulting in a deviation of about 4%.

It is important to mention that a mesh independency is performed for the most critical situations of the cases that will be studied with the highest values of Re and Gr numbers as well as the study of mass conversation due to the use of the penalty method. Just after reaching reasonable results, the final mesh domain and the penalty parameter are used to obtain the final results. All this study can be found in the doctorate thesis of the present author (Guimarães, 2007). It is omitted here as a matter of space.

5. Results

5.1 Case with one heat source

Figure (4) shows the isotherm distributions considering the ranges for the Reynolds number, the Grashof number, and the inclination angle, respectively, as $1 \le Re \le 10$, $10^3 \le Gr \le 10^5$, and $0° \le \gamma \le 90°$. By observing the isotherms from Fig. (4), the orientation of the channel has a more significant effect on the temperature distribution for lower Re, that is, Re = 1, 5, and 10. This effect is even stronger when Gr increases. Later on this chapter, this effect on the Nusselt number will be seen again. On the other hand, for higher Reynolds, over 50 or so (not shown in Fig. (4)), the inclination angle has a weaker effect on the temperature distributions.

Figure (5) shows the effect of the source module on the velocity distributions for the horizontal cases (γ = 0°) with Re = 1, 5, and 10, considering Gr = 10^5. It can be noted that in the natural convection regime, the thermal plume is approximately symmetric about the centerline of the module (Fig. 4). In the thermal plume region, there are two opposite recirculating cells that are almost symmetric. Moreover, as the entrance velocity increases

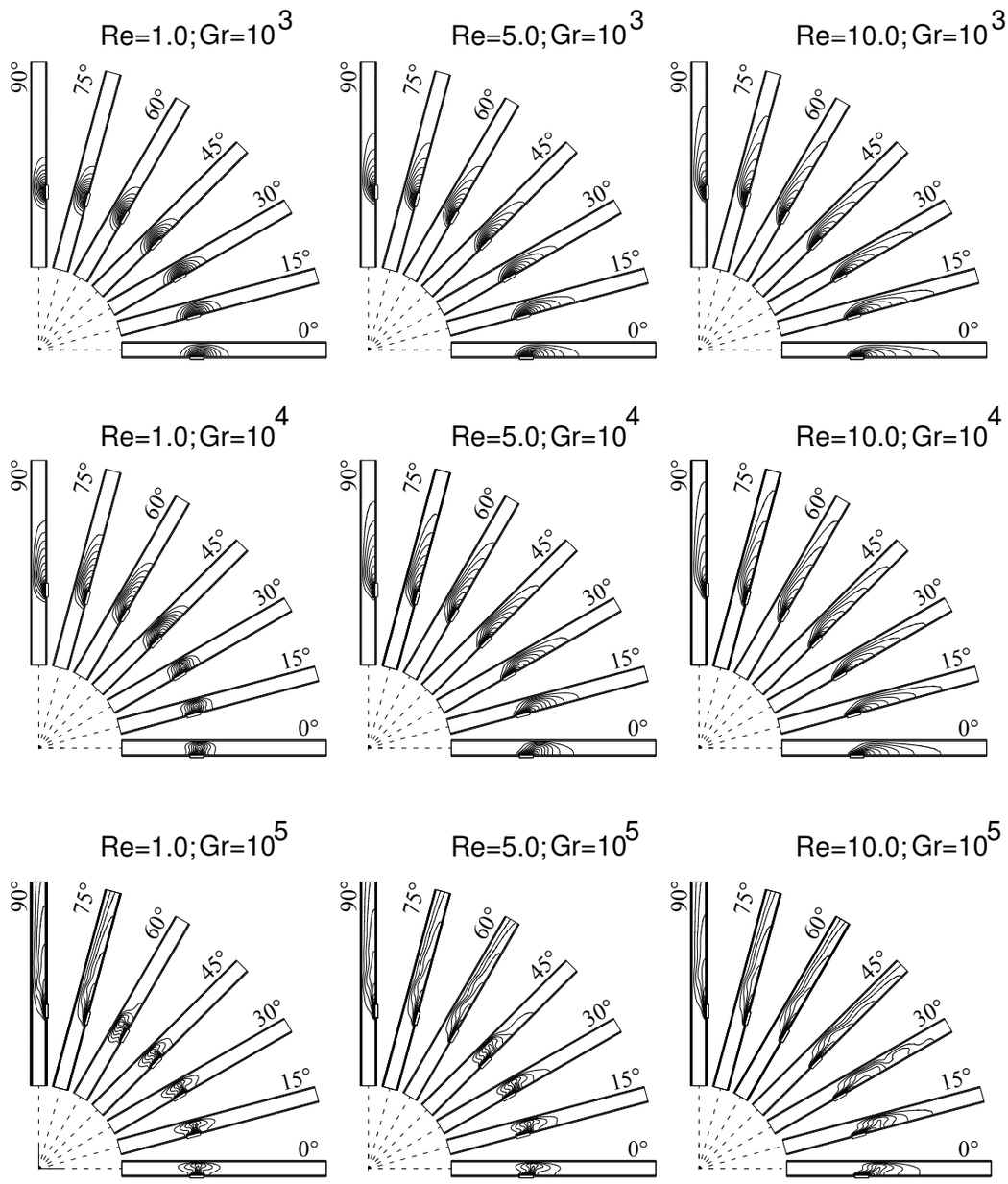

Fig. 4. Isotherms: Gr = 10^3, 10^4, 10^5; Re = 1, 5 , 10; and γ = 0°, 15°, 30°, 45°, 60°, 75°, 90°

the plume shifts and stretches towards downstream. This effect features how the natural convection starts to vanish, giving place to the mixed convection. If Re increases more, for instance, Re ≥ 100 (not shown in Fig. (5)), the forced global fluid movement dominates the flow pattern and the heat transfer process. One can note in the temperature distribution along the module in Fig. (6), for Gr = 10^5, and Re = 1, 5, 10, the transition from the natural convection to the mixed convection. As Re is higher, the maximum temperature on the module decreases. This is due to the fact that when higher velocities are present, the cell recirculation gets further from the module allowing a stronger contact of the cold fluid with the heat module.

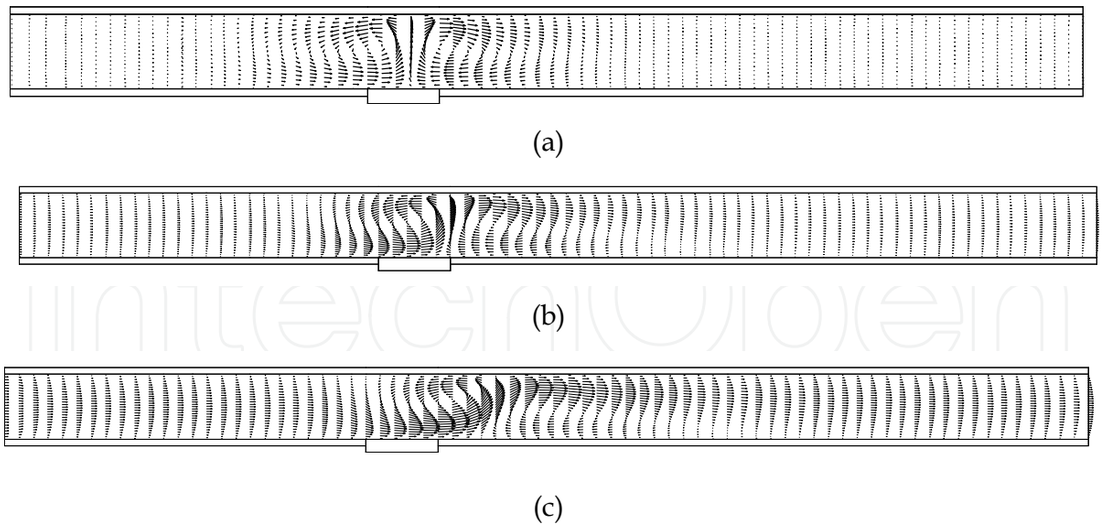

Fig. 5. Velocity distributions for Gr = 10^5, γ = 0°, and Re = (a) 1, (b) 5, and (c) 10

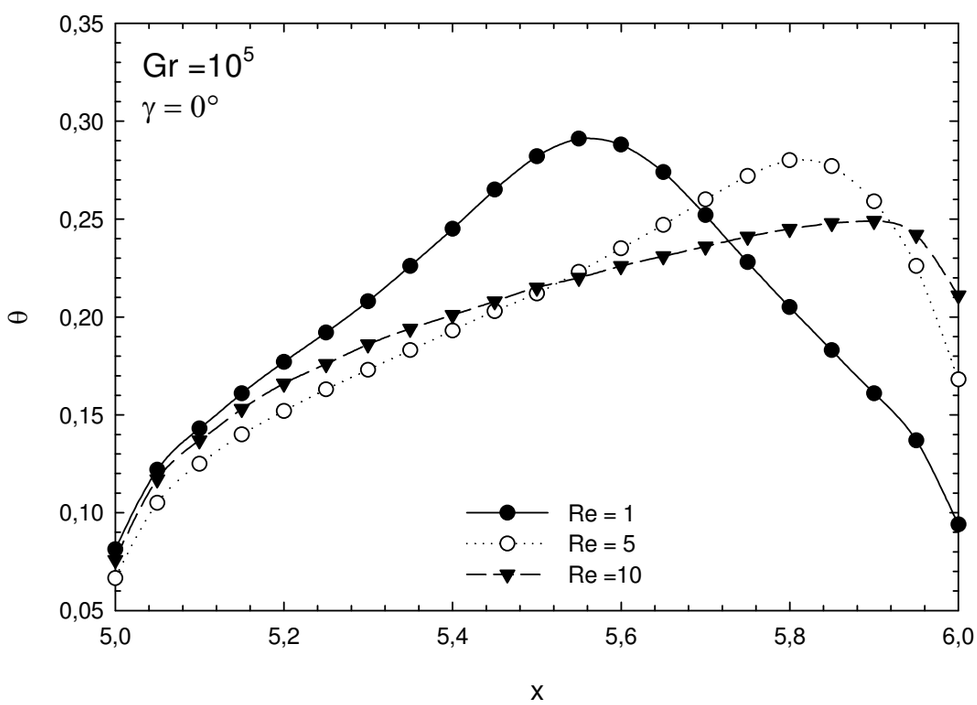

Fig. 6. Module temperature distributions for Gr = 105, γ = 0° and Re = 1, 5, and 10

Figure (7) depicts the velocities vectors for Gr = 10^5 and Re = 1, 5, and 10, for γ = 45°. As Re increases, the clockwise recirculating cell tends to vanish, whereas the anticlockwise ones tend to dominate to an extent that reversed flow exists at the exit. The presence of the reversal flow does not necessarily imply an increase of the Nusselt number on the module. It is interesting to observe the formation of secondary recirculating cells in Fig. (7c), and as a

result of this formation, the corresponding isothermal lines are distorted, as shown in Fig. (4). In Fig. (7b), the reversal flow is weak. Comparing Fig. (7) with Fig. (5), there is a small difference in the velocity vectors, hence showing the small effect of the orientation of the channel in these two cases.

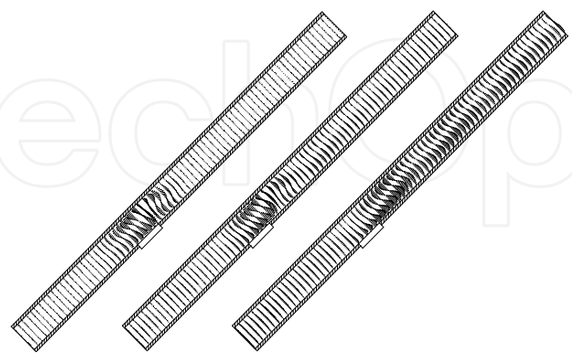

(a) (b) (c)

Fig. 7. Velocity vectors for Gr = 10^5, γ = 45°, and (a) Re =1, (b) Re =5, and (c) Re =10;
Here, γ = 75° is a better situation when cooling is aimed, with little difference when γ = 90°

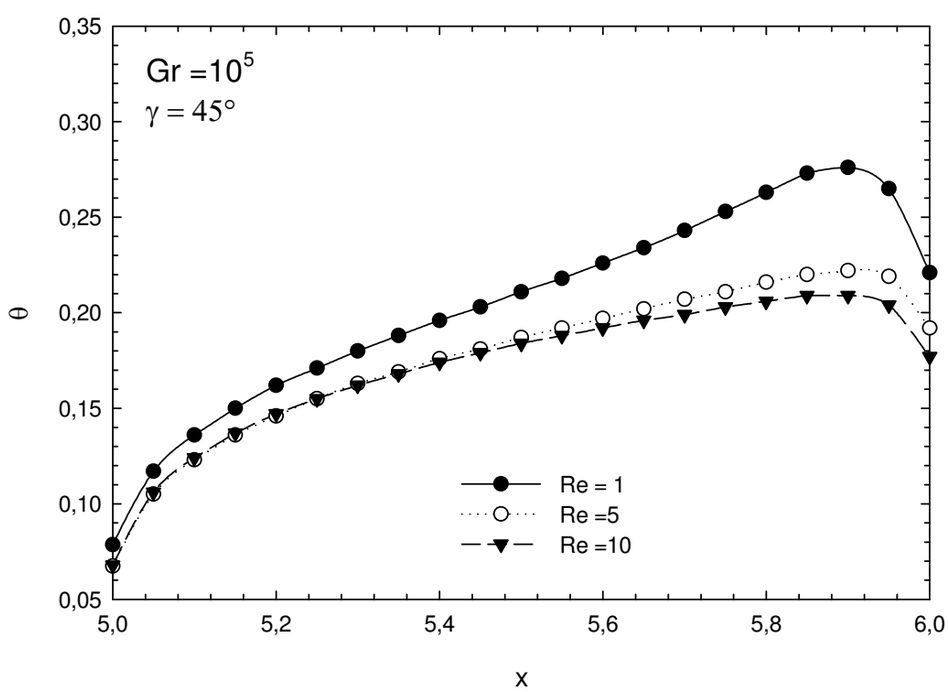

Fig. 8. Module temperature distributions or Gr = 10^5, γ = 45° and Re = 1, 5, and 10

In Figure (8), the temperature distributions along the module are shown for the cases from Fig. (7a-c). In a general way, the maximum temperature on the module decreases for the three cases. It must be remembered that the ideal work conditions in equipments with electronic circuit boards are those in which the module presents the lowest values for the

maximum temperature. Therefore, having these conditions in mind, the increase of the inclination angle provides lower values for the maximum temperature.

Figure (9) presents the velocity distributions for Gr = 10^5, Re = 1, 5, and 10, but now with the channel on the vertical position, $\gamma = 90°$. It can be noted that for all the values of Re, there is a reversal flow at the outlet that is stronger than the reversed flow for $\gamma = 45°$. For each of these three cases in Fig. (9), there is a secondary recirculating cell. There is not a significant difference in the temperature on the module for the Reynolds values Re = 1, 5, and 10; Gr = 10^5, and $\gamma = 90°$(Fig. 10)).

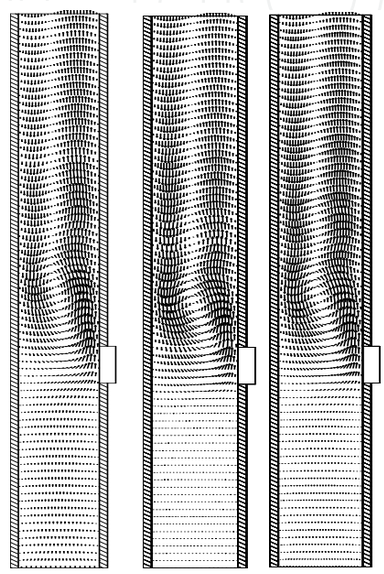

(a) (b) (c)

Fig. 9. Velocity distributions for Gr = 10^5, $\gamma = 90°$, and Re = (a) 1, (b) 5, and (c) 10

Figure (11) makes a comparison of the Nusselt numbers for $1 \leq Re \leq 500$, $0° \leq \gamma \leq 90°$ and for the three Grashof numbers Gr =10^3, 10^4, and 10^5. These results are in good agreement with those found in literature (Choi & Ortega, 1993). It was observed according to the 'five percent deviation rule' (Sparrow et al., 1959) that the natural, mixed, and forced convection can be determined. From Figs. (11a-c), the same is found here, where the mixed convection regimes are, approximately, within the ranges $1 < Re < 50$ for Gr = 10^3, $5 < Re < 100$ for Gr = 10^4, and $10 < Re < 500$ for Gr = 10^5. Practically, there is no reduction in the Nusselt number in these cases where the aiding flow is present, which also agrees with the work previously mentioned (Choi & Ortega, 1993). It can be noted that the collapse of the curves at high Re explains that the buoyancy effects and, therefore, the influence of inclination diminish as forced fluid global motion dominates.

Figure (12) shows the influence of the orientation angle in the heat transfer for all the cases studied in this work, that is, Re from 1 to 500; γ from 0° to 90°; and Gr = 10^3, 10^4, and 10^5. In a general way, Nu is strongly dependent on the orientation of the channel in the limits of the natural and forced convection. For instance, when Gr = 10^3, the natural convective cells are not sufficiently strong to influence the flow and the temperature fields (Fig. 4), that means that the heat transfer mode involved is almost conductive along the channel. As Gr increases, the variations in Nu are more significant for low Re. It is said that in the natural

and mixed convection, the most suitable situation in the cooling of an electronic module, that is, the lowest Nu, is found when the channel orientation is in the range 45°<γ<90° (considering the convention adopted in the present work), in a general way (Choi and Ortega, 1993). Analyzing Fig. (13), there is still a more favorable inclination within the range proposed by previous literature (Choi & Ortega, 1993), which is around 60° and 75°. The case for γ = 0° should be avoided. A particular case which provides a drastic increase in Nu, within the limits considered in this case, is Gr = 10^3 and Re = 1 in the range 60° ≤ γ ≤ 75°. This can also be noted in Fig. (5), in the isotherms distributions.

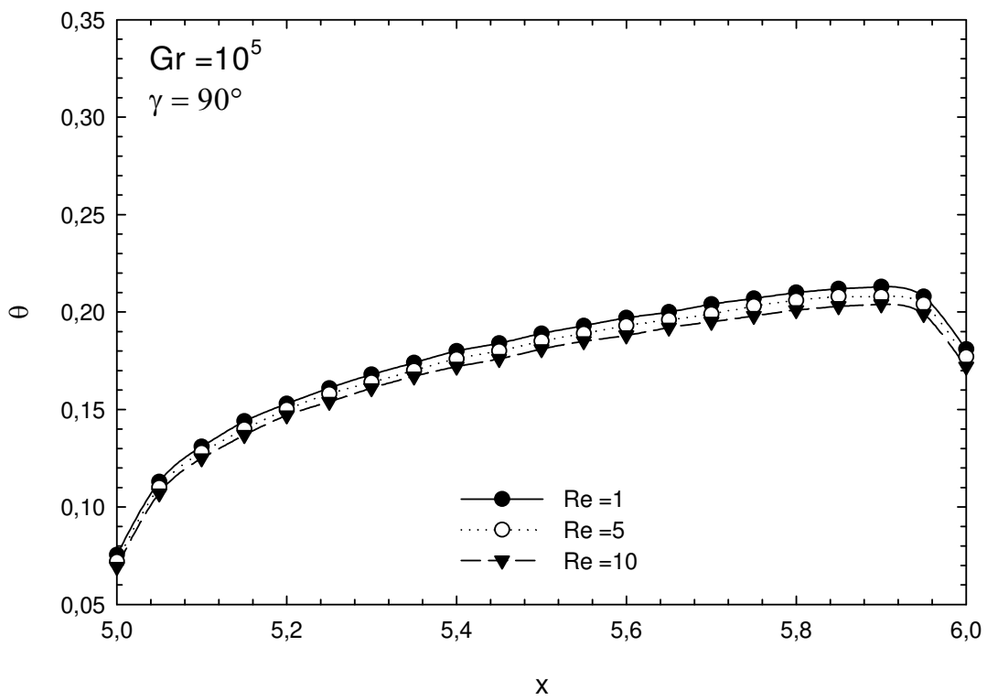

Fig. 10. Module temperature distributions for Gr = 10^5, γ = 90° and Re = 1, 5, and 10

5.2 Case with two heat sources

Figure (13) discloses the velocity vector distributions for Gr = 10^5, Re = 1, 10, and 1000 and d = 1, 2, and 3. In the case where Re = 1, almost symmetric recirculations appear and those are responsible for the thermal plumes mentioned previously. As the source modules are placed further from each other, the recirculation between the sources is powered on and, therefore, higher velocities take part in the flow. For Gr = 10^5, this does not imply a big difference in temperature on the pair of heat sources. In a general way, as Re is raised, the recirculations tend to cease, making it possible to the cold fluid be more in contact with the module surfaces, hence, invigorating the heat transfer. For high values of Re, the distance d has little influence on the velocity profiles. As mentioned before, for Re = 10, an oscillating behavior of the recirculations brought about by the buoyancy flow near the modules is observed. These oscillations reflect an attempt of the flow to be ruled by a predominant convection, that is, it is a 'fight' between buoyant and forced velocities. The first heat source develops a flow wake that hits the second one, heating it even more. The recirculation originated on the second module becomes more intense and this makes an increase in the

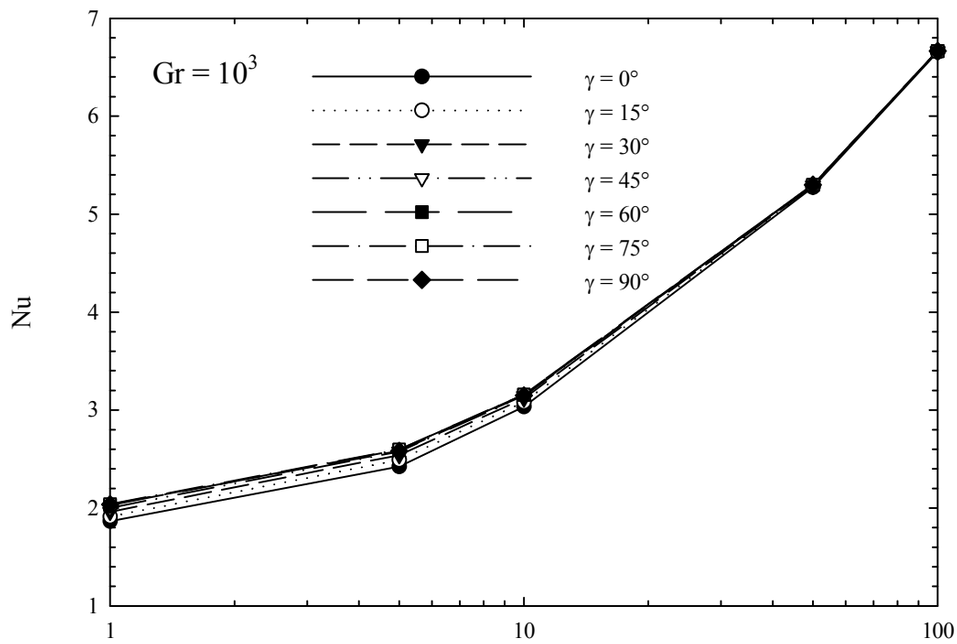
Gr = 10^3
γ = 0°
γ = 15°
γ = 30°
γ = 45°
γ = 60°
γ = 75°
γ = 90°
Nu
1
2
3
4
5
6
7
1
10
100

(a)

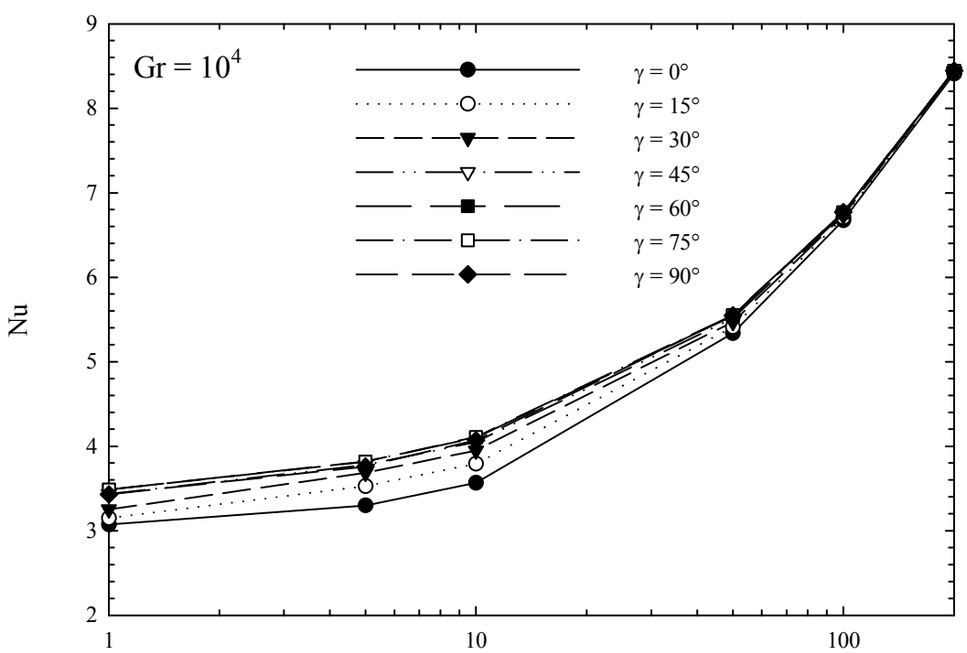
Gr = 10^4
γ = 0°
γ = 15°
γ = 30°
γ = 45°
γ = 60°
γ = 75°
γ = 90°
Nu
2
3
4
5
6
7
8
9
1
10
100

(b)

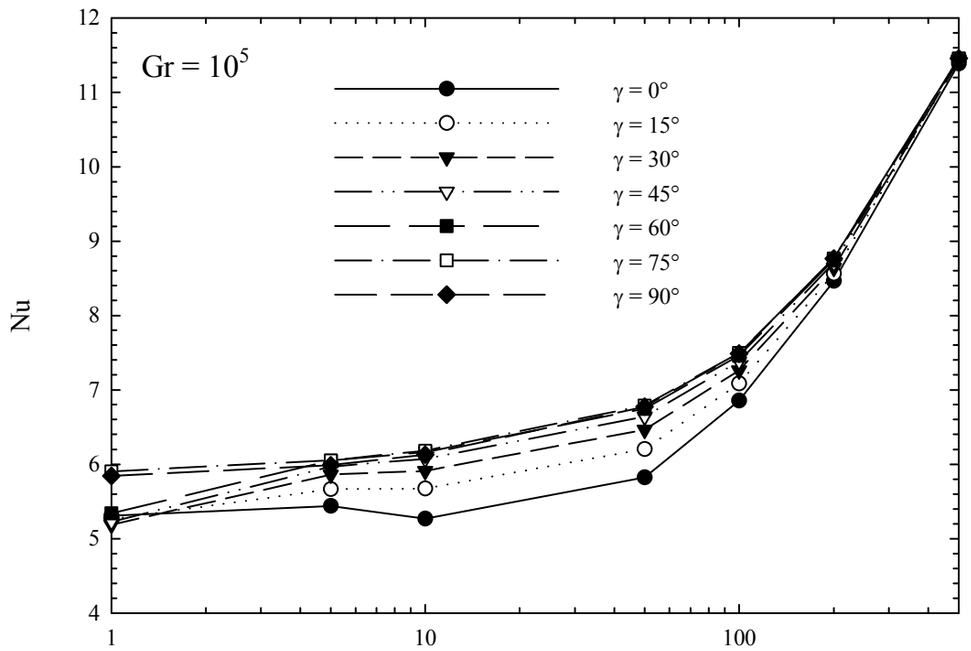

(c)

Fig. 11. Average Nusselt number vs Re: $0 \leq \gamma \leq 90°$, (a) Gr=10^3, (b) Gr= 0^4, and (c) Gr=10^5

fluid pressure coming from backwards. Therefore, it comes to a point that this pressure is strong enough to force that flow barrier downstream. At this moment, the main flow starts to develop and all the process repeats all over again. Consequently, time oscillations in Nu on Heater 2 will appear. This will be seen afterwards.

Figure (14) shows the isotherm distributions for Reynolds numbers Re = 1, 10, 50, 100, and 1000, distances between the heat sources d = 1, 2, and 3 and Grashof number Gr = 10^5. The isotherms are spaced by $\Delta\theta = 0.02$. It can be noted when natural convection is concerned, that is, Re = 1, the heat sources in the cases where d = 1 and 2 influence each other whereas for the case where d = 3, it does not happen. For all cases where Re = 1, there are plumes localized in the vicinity of the heaters. For Re = 1 and d = 1, the two plumes are partially glued, making it clear that this distance does make the module temperature fields impact each other. Although this is also true when d = 2, the plumes are further spaced from each other. For Re = 1 and d = 3, the plumes are almost independent. It will be seen that this behavior in Heater 1 and Re = 1 affects smoothly the Nusselt number Nu when Gr = 10^5. Moreover, for Gr = 10^3 and 10^4, the space between the modules does not interfere on heat transfer. On the other hand, when Heater 2 is taken into consideration, the heat source spacing invigorates Nu for Gr = 10^3, 10^4, and 10^5. A perfect symmetry is not present here as long as the flow has a certain forced velocity, Re = 1, in the forced stream. For all Reynolds numbers and Gr = 10^5, the solutions converge. However, for Re = 10, a periodic flow oscillation in time is brought about for all heat source distances. The temperature distributions (not shown here) where Re = 10 and d = 1, 2, and 3 are plotted in the time shots t = 15, 30, and 50, respectively. It can be perceived in these cases, higher temperature distribution on the second module. This temperature rise tends to weaken as the Reynolds number is increased. The temperature invigoration in the region around Heater 2 is due to the fact that the thermal wake from Heater 1 intensifies the buoyant flow in the localized region in the vicinity of Heater 2. It can be noted that by keeping Re constant, the distance d

plays a considerable role on the second module heating. For instance, what has just been said happens in the case where Re = 1000 and d = 1, 2, and 3.

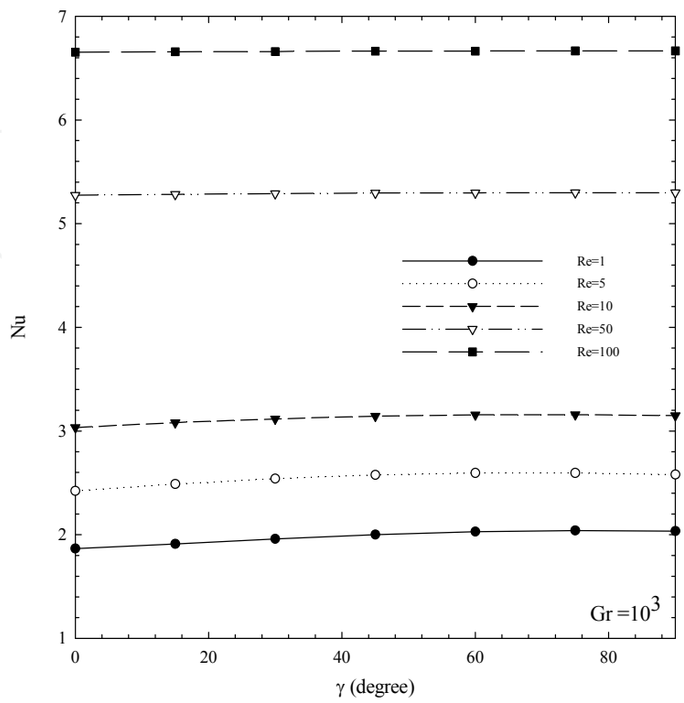

(a)

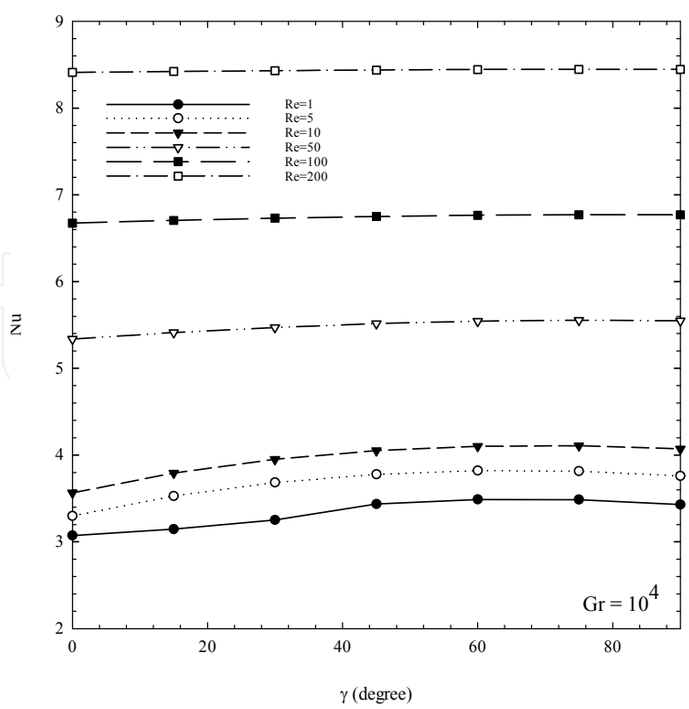

(b)

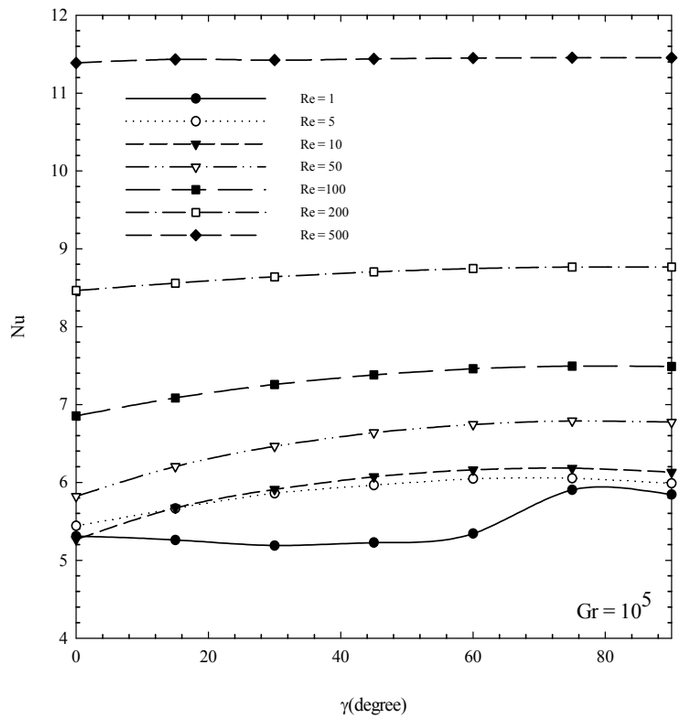

(c)

Fig. 12. Average Nusselt vs γ: 1 ≤ Re ≤ 500 and (a) Gr = 10^3, (b) Gr = 10^4, and (c) Gr = 10^5

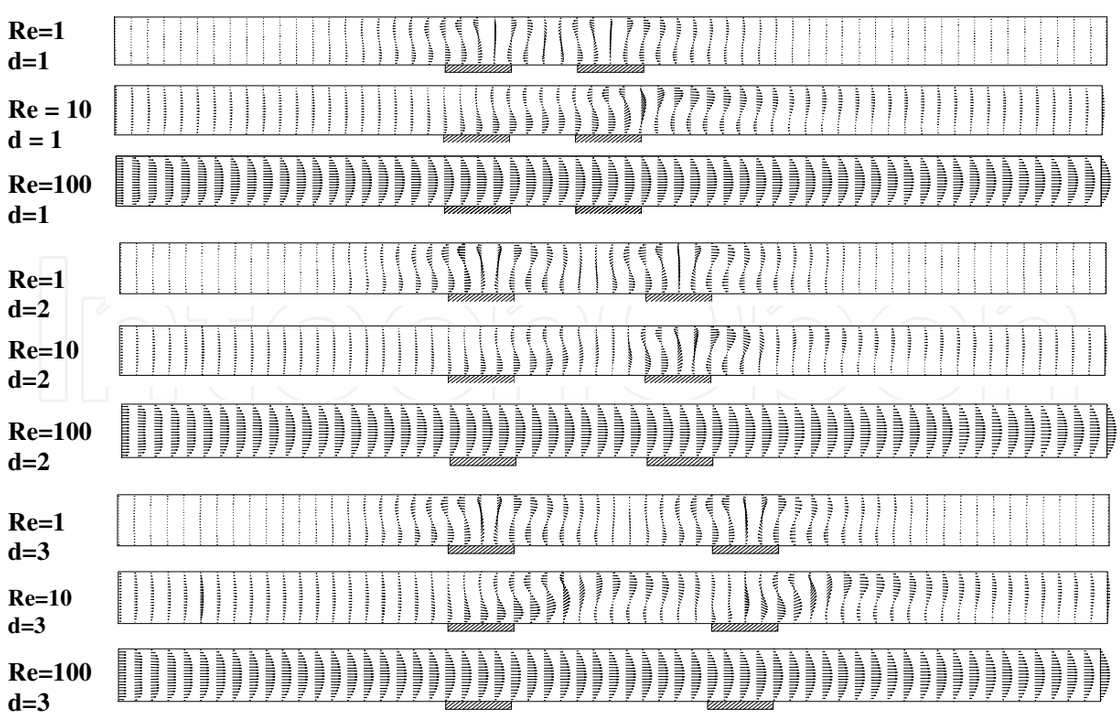

Fig. 13. Velocity vector for Gr = 10^5, Re = 1, 10, 100, and d = 1, 2, 3

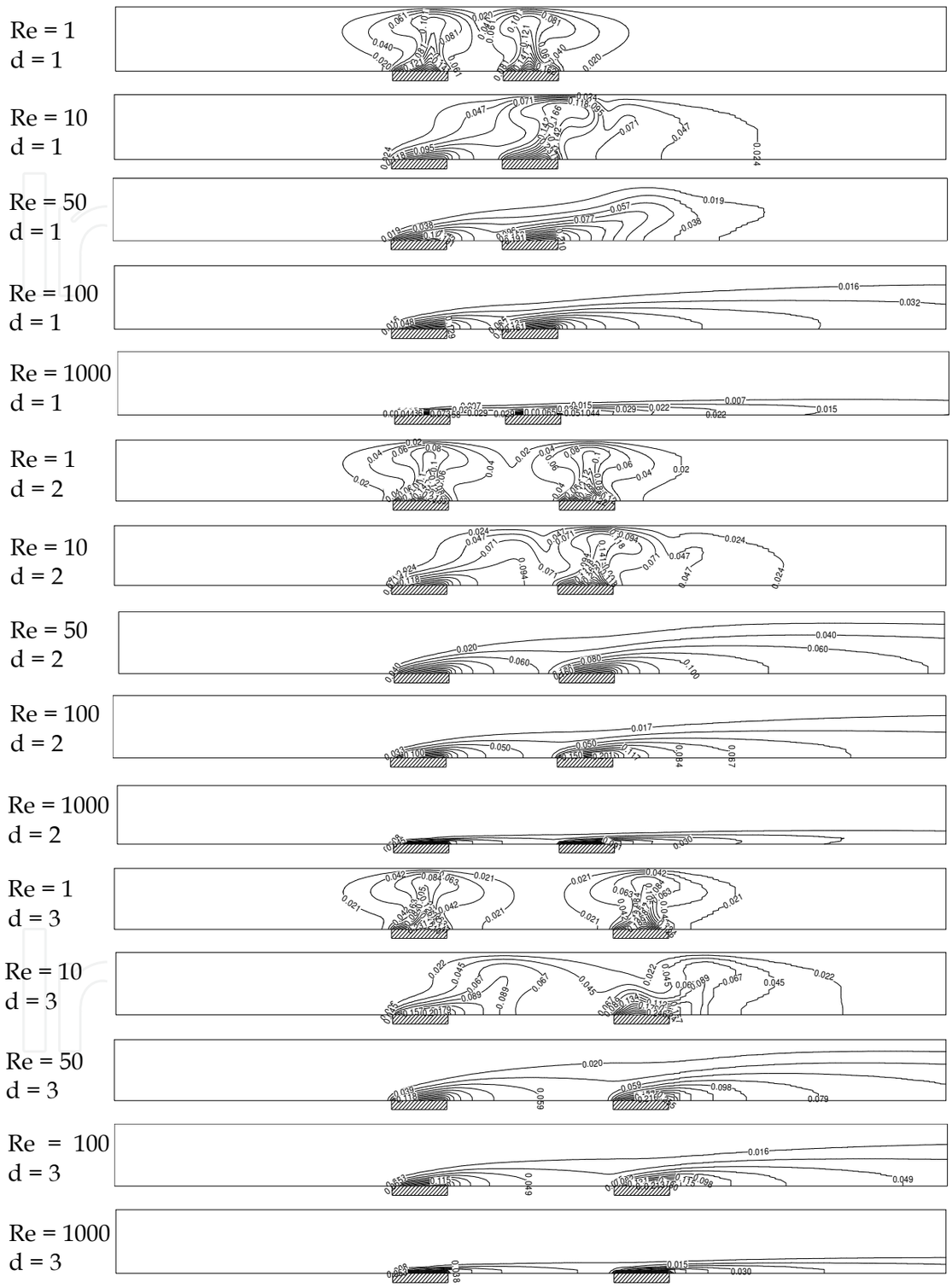

Fig. 14. Isotherms for Re = 1, 10, 100, 1000, $\gamma = 0°$, and Gr = 10^5, $\Delta\theta = 0.02$

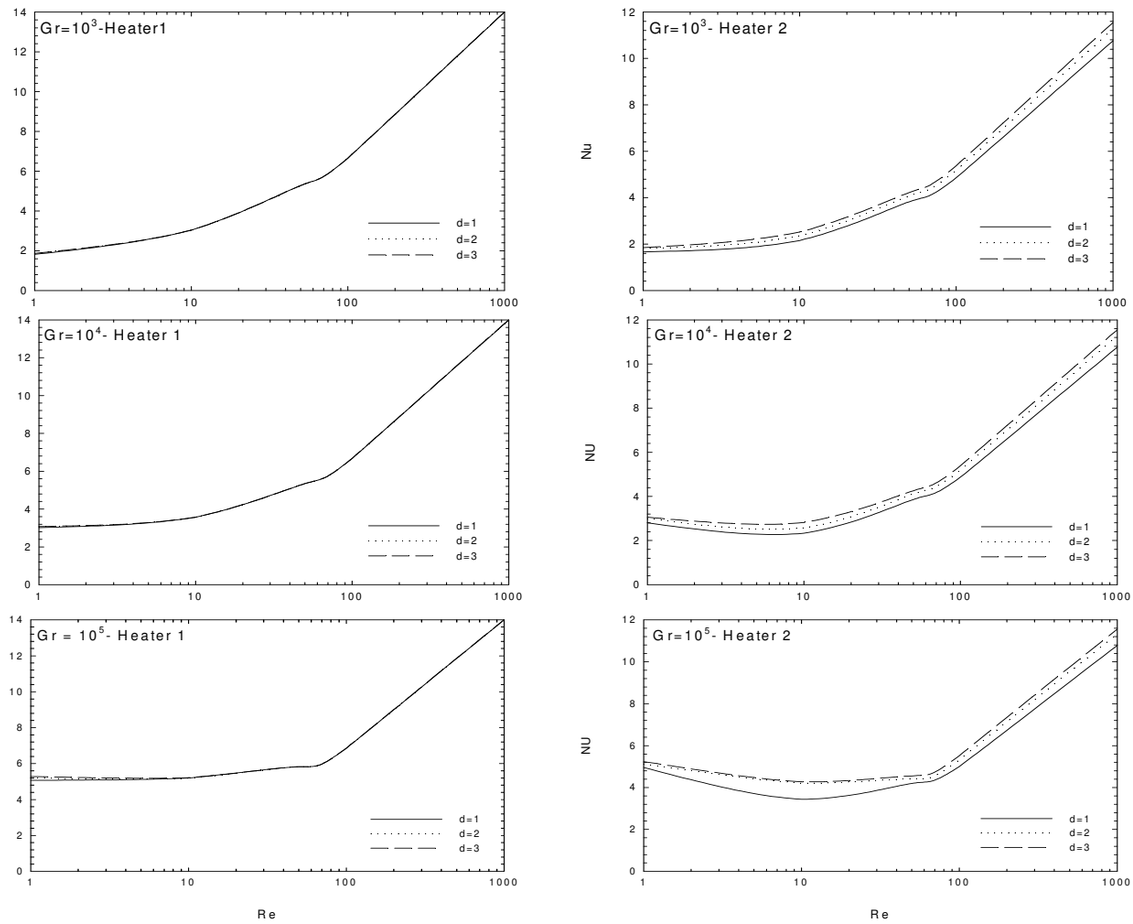

Fig. 15. Nu for Re = 1, 10, 10^2, 10^3, d = 1, 2, 3, Gr = 10^5, 10^4, and 10^5 on Heater 1 and 2

Figure (15) depicts the effect of the Reynolds number on heat transfer for Gr = 10^3, 10^4, and 10^5, Re = 1, 10, 100, and 1000, and finally, d = 1, 2, 3, in the pair of heat sources. This picture shows some points already discussed previously such as the module distance effect which is almost negligible on Heater 1 and moderate on Heater 2. It can be clearly seen the balance between forced and natural convections. In a general way, the distance d = 3 is the one which offers better work conditions since the temperatures are lower.

Figure (16) presents the temperature distributions θ on Heater 1 and 2 for Re = 100 and 1000 and d = 1, 2, and 3. The distance between the modules does not affect the temperature on Heater 1 whereas this effect can be distinctively seen on Heater 2. It is interesting noticing in Heater 2, that for Re = 100 and 1000, distances d = 2 and 3 do not present significant changes, but d = 1. Then, there is an optimum distance in which two heat sources can be placed apart to have lower temperatures and this is the case of d = 3 here, although d = 2 does not present a meaningful change in temperature either. This, in a certain way, can lead us to a better layout of the heat sources in an array. Of course, the presence of more heat sources and the geometry of the channel must be taken into account. Anyway, this behavior is food for thought for future studies.

Finally, the time distribution of the Nusselt number along Heater 1 and 2 for Gr = 10^5, Re = 10, 100, and 1000, d = 1, 2, and 3, is shown in Fig. (17). In all cases, as expected, the first

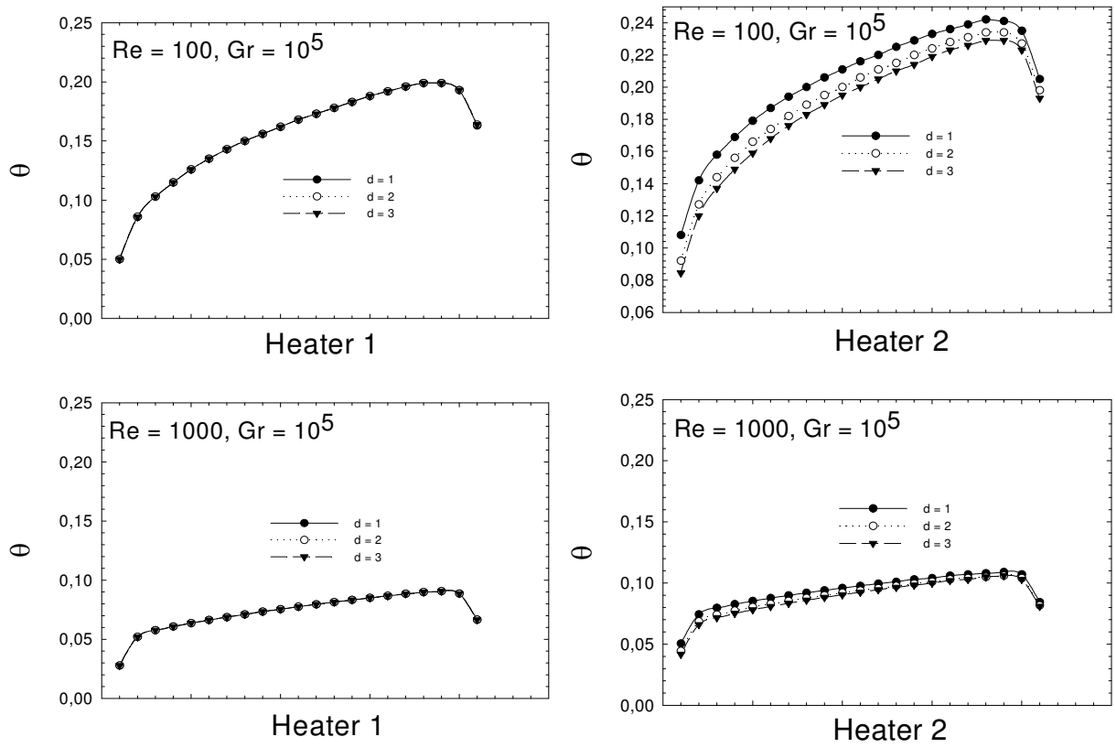

Fig. 16. Temperature on modules 1 and 2 for d = 1, 2, 3; Re = 100, 1000, and Gr = 10^5

module is submitted to higher heat transfer since it is constantly been bombarded with cold fluid from the forced convection. On the other hand, it can be seen again that a flow wake from the first source reaches the second one and this is responsible for the bifurcation of the Nusselt number curves. Here, one can note the time spent by the hot fluid coming from the first source and traveling to the second one. For example, for Re = 100 and d = 1, 2, and 3, the time shots are, respectively, around t = 1.4, 3.0, and 4.0. However, the converged values for these last cases are almost the same. As seen earlier, periodic oscillations appear for Re = 10.

5.3 Case with three heat sources

The results presented here are obtained using the finite element method (FEM) and a structured mesh with rectangular isoparametric four-node elements in which $\Delta X = 0.1$ and $\Delta Y = 0.05$. A mesh sensibility analysis was carried out (Guimaraes, 2008). The temperature distributions for Reynolds numbers Re = 1, 10, 50, and 100, Grashof number Gr = 10^5, and inclination angles $\gamma = 0°$ (horizontal), 45°, and 90° (vertical) are available in Fig. (18). For Re = 1 and $\gamma = 0°$ and 45°, there is a formation of thermal cells which are localized in regions close to the modules. When Re = 1, the flow is predominantly due to natural convection. As Re is increased, these cells are stretched and hence forced convection starts to be characterized. By keeping Re constant, the inclination angle variation plays an important role on the temperature distribution. The effect of γ on temperature is stronger when low velocities are present. For example, when Re = 10 and $\gamma = 0°$, 45° and 90°, this behavior is noted, that is, for $\gamma = 0°$ and Re = 10, a thermal cell is almost present, however, for $\gamma = 45°$and Re = 10, those cells vanish. This is more evident when Re =1 and $\gamma = 45°$ and 90°.

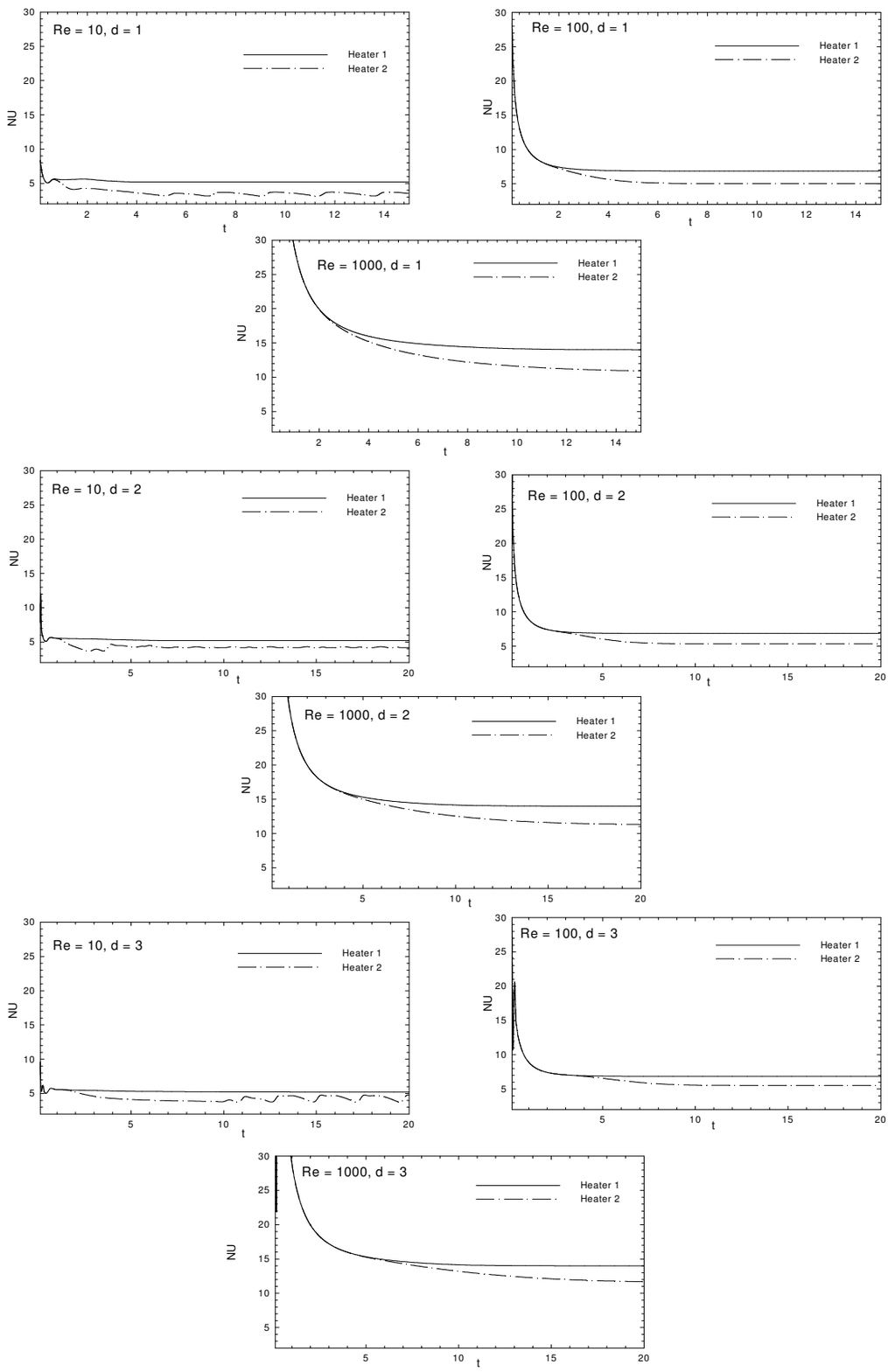

Fig. 17. Average Nusselt number vs Time: Gr = 10^5, Re = 10, 10^2, 10^3, d =1, 2 , 3, Heater 1, 2

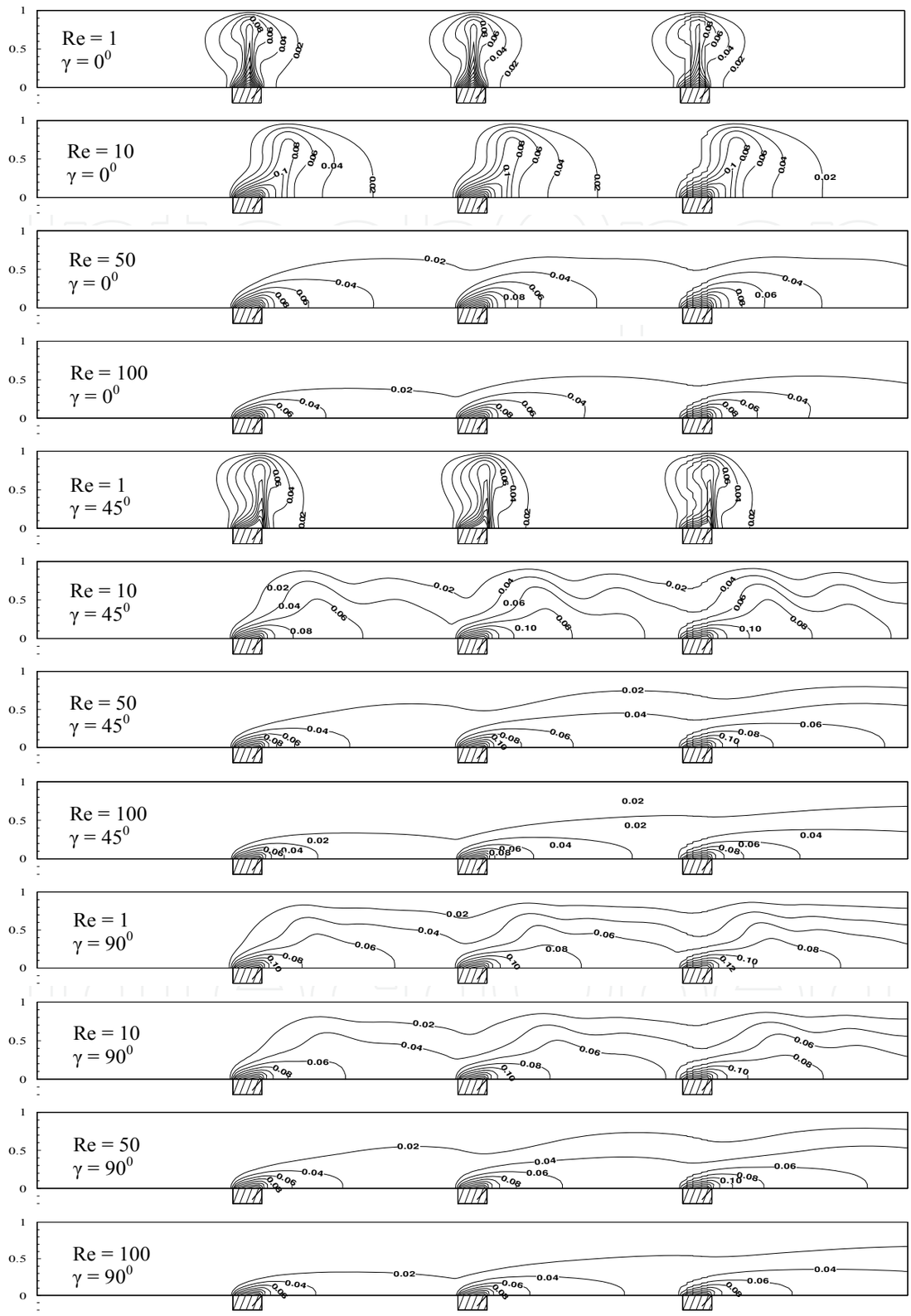

Fig. 18. Isotherms for Gr = 10^5, Re = 1, 10, 50, 100 and γ = 0°, 45°, 90°

It is worth observing that, the fluid heated in the first heater reaches the second one, and then the third one. Thus, this process of increasing temperature provides undesirable situations when cooling is aimed.

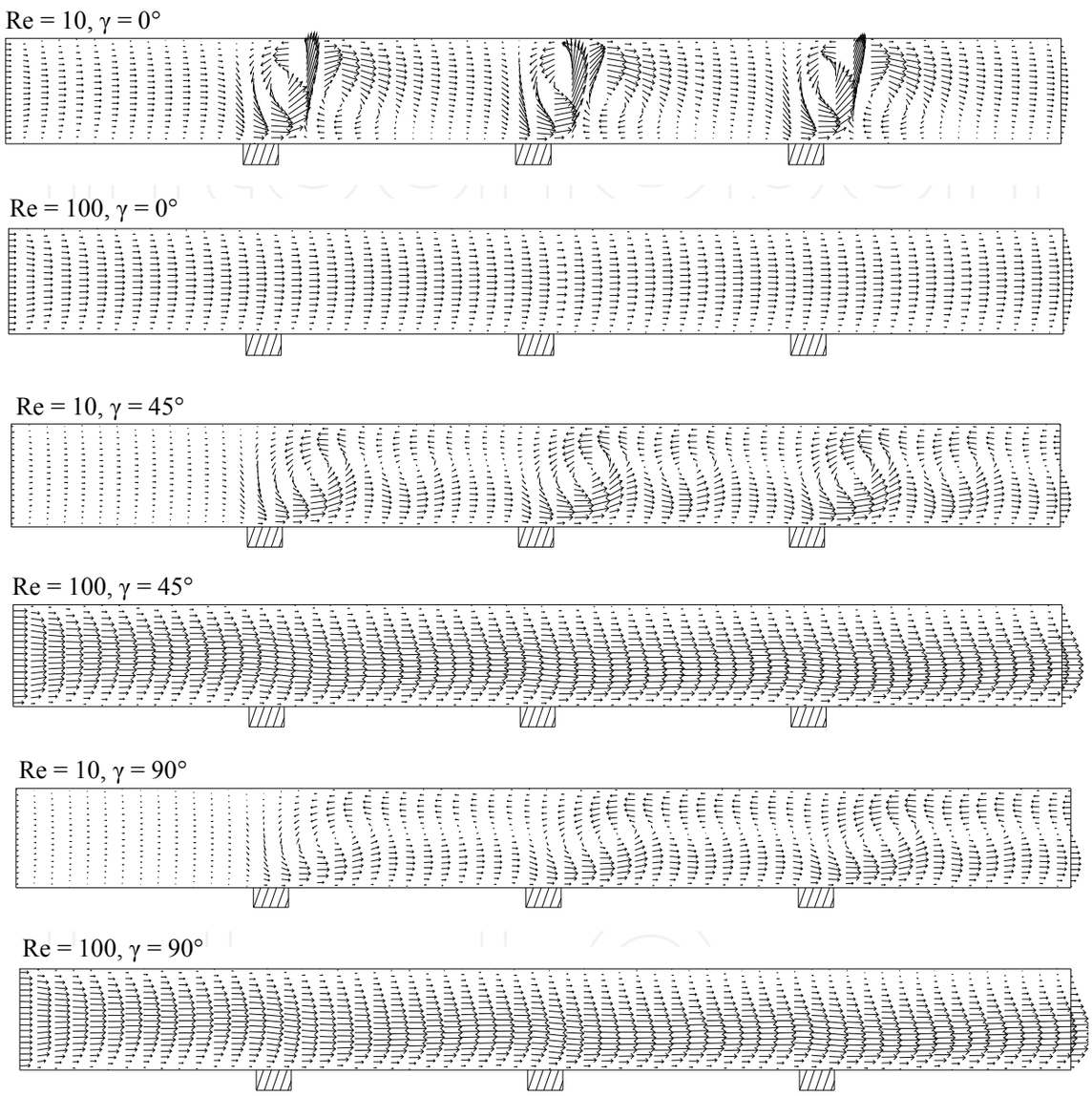

Fig. 19. Velocity vectors for Gr = 105, Re = 10 and 100, and γ = 0°, 45°and 90°

Figure (19) depicts the velocity vectors for Re = 10 and 100 and Gr = 10^5 for γ = 0°, 45°, and 90°. It can be noted that for Re = 10 and γ = 0°, 45°, and 90°, recirculations are generated by the fluid heated on the sources. For Re = 10 and γ = 0°, three independent recirculations appear. The distance among the heat sources enables the reorganization of the velocity profile until the fluid reaches the next source and then the recirculation process starts all over again. Now, concerning the cases where Re = 10 and γ = 45° and 90°, there are two kinds of recirculations, that is, a primary recirculation along all channel that encompasses

another two secondary recirculations localized just after the sources. Moreover, for these later cases, a reversal fluid flow is present at the outlet. As Re is increased by keeping γ constant, these recirculations get weaker until they disappear for high Re. Clearly, one can note the effect of the inclination on the velocity vectors when Re = 10. The strongest inclination influence takes place when it is between 0° and 45°.

Figure (20) presents the average Nusselt number distributions on the heat sources, NU_{H1}, NU_{H2}, and NU_{H3} for Reynolds numbers Re = 1, 10, 50, 100, and 1000, Grashof numbers Gr = 10^3, 10^4, and 10^5, and inclination angles γ = 0°, 45°, and 90°. In general, the average Nusselt number for each source increases as the Reynolds number is increased. By analyzing each graphic separately, it can be observed that NU_{H1} tends to become more distant from NU_{H2} and NU_{H3} as Reynolds number is increased, starting from an initial value for Re = 1 which is almost equal to NU_{H2} and NU_{H3}. This agreement at the beginning means that the heaters are not affecting one another. Here, it can be better perceived that behavior found in Fig. (13), where a heater is affected by an upstream one. That is the reason why NU_{H1} shows higher values. The only case in which the heaters show different values for Re = 1 is when Gr = 10^5 and γ = 90°. Overall, the strongest average Nusselt number variation is between 0° and 45°. Practically in all cases, NU_{H1}, NU_{H2} ,and NU_{H3} increase in this angle range, 0° and 45°, while for Gr = 10^5 and Re = 1000, NU_{H2} and NU_{H3} decrease. When electronic circuits are concerned, the ideal case is the one which has the highest Nusselt number. Thus, angles 45° and 90° are the most suitable ones with not so

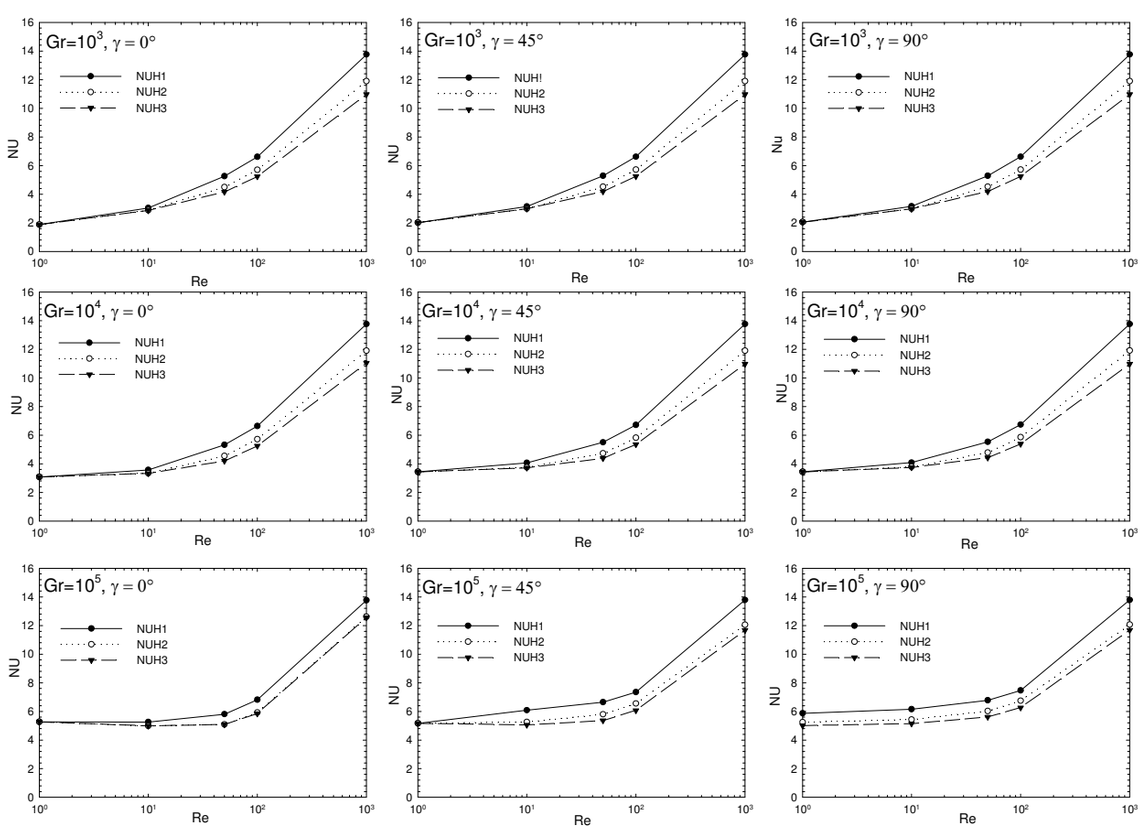

Fig. 20. Average Nusselt number vs Reynolds number for Gr = 10^3, 10^4, 10^5, γ = 0°, 45°, 90°

much difference between them. An exception would be the case where Gr = 10^5, Re = 1000, and $\gamma = 0°$.

Figure (21) presents the local dimensionless temperature distributions on the three heat sources for Re = 10, 100, 1000, Gr = 10^5, $\gamma = 0°$, 45°, and 90°. Again, the cases where Re = 10 and 100 show the lowest temperatures when $\gamma = 90°$. On the other hand, this does not happen when Re = 1000, where the horizontal position shows the lowest temperatures along the modules. All cases in which $\gamma = 0°$, the second and third sources have equal temperatures. However, the first module shows lower temperatures. As mentioned before, this characterizes the fluid being heated by a previous heat source, thus, not contributing to the cooling of an upstream one.

Figure (22) presents the average Nusselt number variation on H_1, H_2, and H_3 against the dimensionless time t considering Re = 10, 100, Gr = 10^3, 10^4, 10^5 and $\gamma = 90°$. In the beginning, all three Nusselt numbers on H_1, H_2, and H_3 have the same behavior and value. These numbers tend to converge to different values as time goes on. However, before they do so, they bifurcate at a certain point. This denotes the moment when a heated fluid wake from a previous source reaches a downstream one.

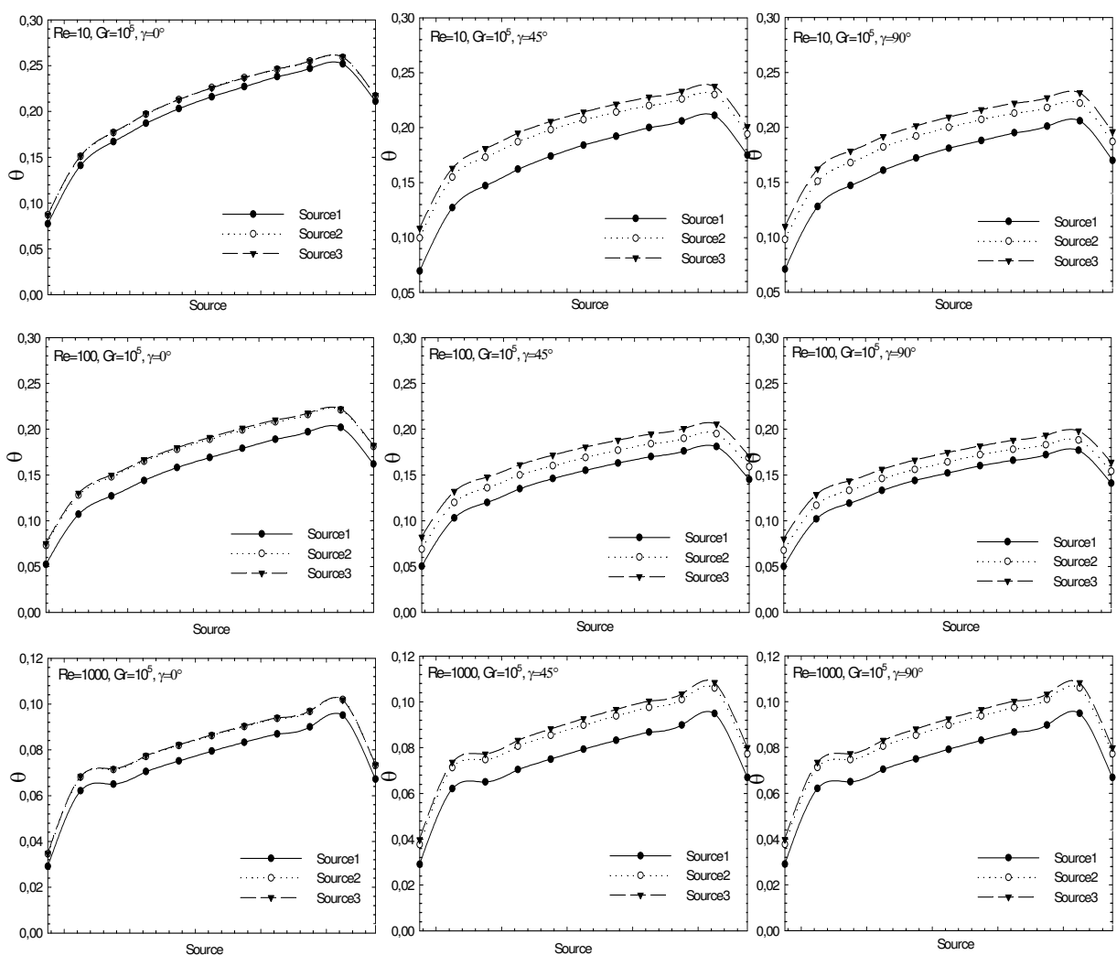

Fig. 21. Module temperatures for Re = 10, 100, 1000; Gr = 105, $\gamma = 0°$, 45°, 90°

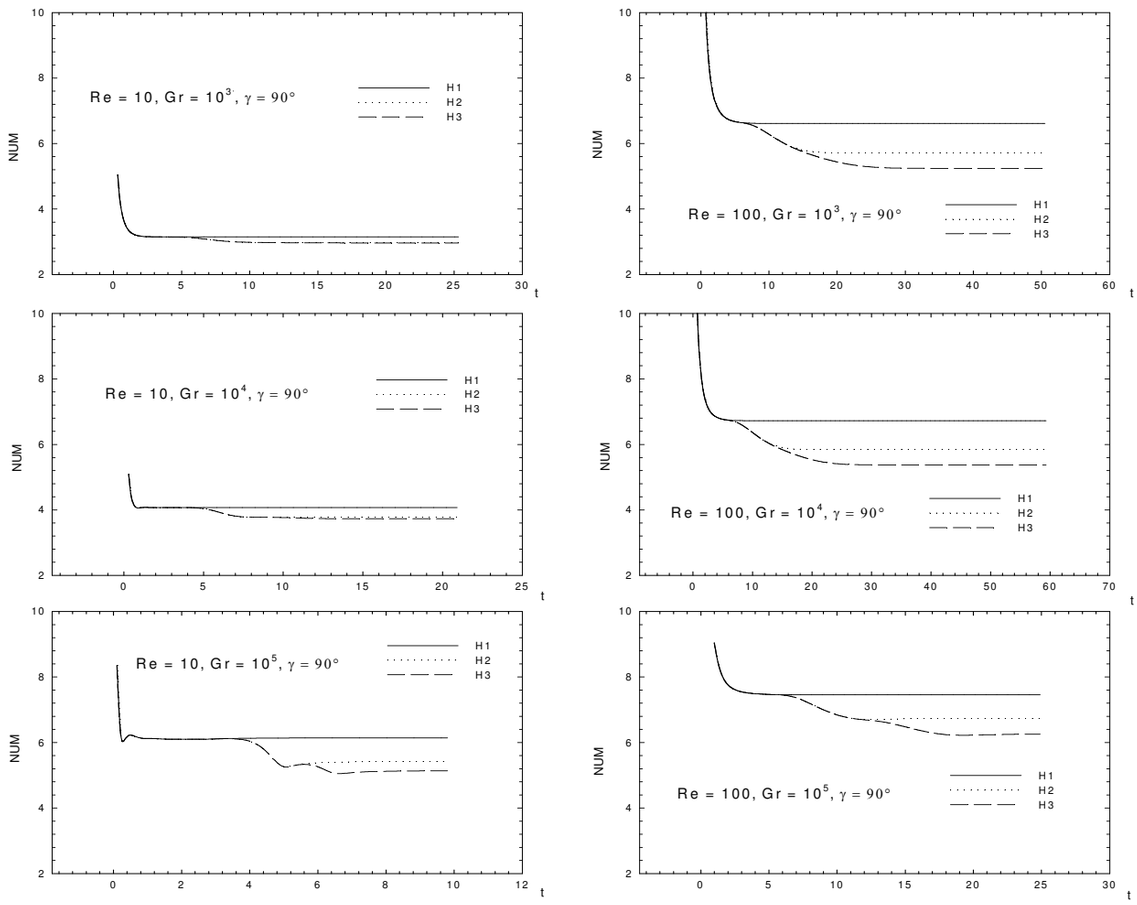

Fig. 22. Module average Nusselt number in time: Re = 10 e 100 , Gr = 10^3, 10^4, 10^5, $\gamma = 90°$

6. Conclusions

1. The mixed convection was studied in a simple channel considering the effect of the inclination angle and some physical parameters. The ranges performed were as follows: $1 \leq Re \leq 500$, $10^3 \leq Gr \leq 10^5$, and $0° \leq \gamma \leq 90°$. The set of governing equations were discretized and solved using the Galerkin finite element method (FEM) with the Penalty formulation in the pressure terms and the Petrov-Galerkin perturbations in the convective terms in all throughout the chapter. 5980 four-noded elements were used to discretize the spatial domain. Comparisons were performed to validate the computational code. It was observed from the results of the present problem that the effect of the inclination angle on the velocity and temperature distributions plays an important role on the heat transfer for low Re and high Gr. For high Re, the effect of the orientation was negligible. One must understand that when the words 'low' and 'high' were mentioned here, it meant low and high compared to the limits considered in this work. In general, it was also discovered that an inclination angle around 60° and 75° provided a slight most desirable work conditions when cooling is aimed. It was said that this optimal orientation would be 90° (Choi and Ortega, 1993), despite no significant changes were found after $\gamma = 45°$ (according to the convection adopted here).

Some cases presented the reversed flow for low Re and high Gr. The reversal flow did not noticeably influence the heat transfer coefficient on the module, although it did change the velocity and temperature fields.

In general, the results encourage the use of inclined boards in cabinets. However, some other aspects should be addressed such as the geometrical arrangement of the boards.

2. A mixed convection study in a rectangular channel with two heat sources on the bottom wall was conducted. The upper wall was kept at a constant cold temperature and the remaining part of the lower one was adiabatic. The heat transfer was studied by ranging some physical and geometrical parameters as follows: Re = 1 to 1000; the distances between the modules d = 1, 2, and 3; and Gr = 10^3, 10^4, and 10^5. For Re = 1 and distances d = 1 and 2, the buoyant forces generated plumes that interfered in each other. For higher Reynolds numbers, the heat transfer in Heater 2 was invigorated by a hot wake brought about by Heater 1. In cases where Re = 10 and Gr = 10^5, the flow oscillations appeared and they strongly affected the flow distributions. For Re = 100 and 1000, the temperature distributions in Heater 1 were not affected by the distances between the modules whereas on Heater 2, they were distinct. An important conclusion is that there was an optimum distance in which two sources could be placed apart from each other, that is, d = 3, although d = 2 did not present a significant change in temperature either. Further investigations are encouraged taking into consideration more heaters and different arrays.
3. In this work, mixed convection heat transfer study in an inclined rectangular channel with three heat sources on the lower wall was carried out using the same. Effects on the Nusselt number along the heat sources as well as the velocity vectors in the domain were verified by varying the following parameters: γ = 0°, 45°, 90°, Re = 1, 10, 50, 100, 1000, Gr = 10^3, 10^4, 10^5. In general, the inclination angle had a stronger influence on the flow and heat transfer since lower forced velocities were present, especially when the channel was between 0° and 45°. It could be noted that in some cases some heat sources were reached by a hot wake coming from a previous module, thus, increasing their temperatures. Primary and secondary recirculations and reversal flow were present in some situations such as Re = 10, γ = 45° and 90°. In problems where heat transfer analysis on electronic circuits is aimed, cases with the lowest temperatures, and hence, the highest Nusselt numbers, are the most suitable ones. Therefore, the channel inclination angles 45° and 90° were the best ones with little difference between them. An exception was the case with Gr = 10^5 and Re = 1000, where γ = 0° was the ideal inclination.

The authors found an interesting behaviour in all three cases with one, two or three heat sources: There is a moment in all three cases studied when oscillations in time near the heat sources appear, featuring their initial strength and then reaching its maximum and, eventually, ending up going weaker until the flow does not present these time oscillations anymore. This is a very interesting physical moment that a certain dimensionless number may be created or applied in order to feature this behaviour at its maximum or its appearance length in time. However, this will be left for future works from the same authors or from new authors.

7. Acknowledgment

The authors thank the following Brazilian support entities: CAPES, CNPq, and FAPEMIG.

8. References

Arquis, E.; Rady M.A.; Nada, S.A. (2007). A numerical investigation and parametric study of cooling an array of multiple protruding heat sources by a laminar slot air jet, *International Journal of Heat and Fluid Flow*, Vol. 28, pp. 787–805.

Madhusudhana Rao, G. & Narasimham, G.S.V.L. (2007). Laminar conjugate mixed convection in a vertical channel with heat generating components, *International Journal of Heat and Mass Transfer*, Vol. 50, pp. 3561–3574.

Muftuoglu, A. & Bilgen E. (2007). Conjugate heat transfer in open cavities with a discrete heater at its optimized position, *International Journal of Heat and Mass Transfer*, doi:10.1016/j.ijheatmasstransfer.2007.04.017.

Premachandran, B. & Balaji C. (2006). Conjugate mixed convection with surface radiation from a horizontal channel with protruding heat sources, *International Journal of Heat and Mass Transfer*, Vol. 49, pp. 3568–3582.

Dogan, A.; Sivrioglu, M.; Baskaya S. (2005). Experimental investigation of mixed convection heat transfer in a rectangular channel with discrete heat sources at the top and at the bottom, *International Communications in Heat and Mass Transfer*, Vol. 32, pp. 1244–1252.

Binet, B. & Lacroix, M. (2000). Melting from heat sources flush mounted on a conducting vertical wall, *Int. J. of Numerical Methods for Heat and Fluid Flow, Vol.* 10, pp. 286–306.

Baskaya, S.; Erturhan, U.; Sivrioglu, M. (2005). An experimental study on convection heat transfer from an array of discrete heat sources, *Int. Comm. in Heat and Mass Transfer*, Vol. 32, pp. 248–257.

Da Silva, A.K.; Lorente, S.; Bejan, A. (2004). Optimal distribution of discrete heat sources on a plate with laminar forced convection, *International Journal of Heat and Mass Transfer*, Vol. 47, pp. 2139–2148.

Heinrich, J. C. & Pepper, D. W. (1999). Intermediate Finite Element Method. Ed. Taylor & Francis, USA.

Bae, J.H. & Hyun, J.M. (2003). Time-dependent buoyant convection in an enclosure with discrete heat sources, *Int. J. Thermal Sciences*.

Madhavan, P.N. & Sastri, V.M.K. (2000). Conjugate natural convection cooling of protruding heat sources mounted on a substrate placed inside an enclosure: a parametric study, *Comput. Methods Appl. Mech Engrg.*, Vol. 188, pp. 187-202.

Choi, C.Y. & Ortega, A. (1979). Mixed Convection in an Inclined Channel With a Discrete Heat Source, *International Journal of Heat and Mass Transfer*, Vol. 36, pp. 3119-3134.

Bercovier, M. & Engelman, M. (1979). A Finite Element for the Numerical Solution of Viscous Incompressible Flow, *J. Comput. Phys.*, Vol. 30, pp. 181-201.

Carey, G. F. & Krishnam (1982). Penalty Approximation of Stokes Flow, *Comput. Methods Appl. Mech. Eng.*, Vol. 35, pp. 169-206.

Lee, T. & Mateescu, D. (1988). Experimental and Numerical Investigation of 2-D Backward-Facing Step Flow, *J. Fluids and Structures*, Vol. 12, pp. 703-716.

Armaly, B. F.; Durst, F; Pereira, J.C.F. & Schonung, B. (1983). Experimental and Theoretical Investigation of Backward-Facing Step Flow, *J. Fluid Mech.*, Vol. 127, pp. 473-496.

Gartling, D.K. (1990). A Test Problem for Outflow Boundary Conditions – Flow over a Backward-Facing Step, *Int. J. Num. Meth. in Fluids*, Vol. 11, pp. 953-967.

Kim, J. & Moin, P. (1985). Application of a Fractional-Step Method to Incompressible Navier-Stokes Equations, *J. Comp. Physics*, Vol. 59, pp. 308-323.

Sohn, J. (1988). Evaluation of FIDAP on Some Classical Laminar and Turbulent Benchmarks, *Int. J. Num. Meth. in Fluids*, Vol. 8, pp. 1469-1490.

Comini, G.; Manzam, M. & Cortella, G.. Open Boundary Conditions for the Streamfunction –Vorticity Formulation of Unsteady Laminar Convection, *Num. Heat Transfer Part B,* Vol. 31, pp. 217-234.

Guimarães, P.M. (2007). Phd. Thesis: Heat transfer analysis of mixed convection using the Petrov-Galerkin technique and the penalty, Brazil.

Guimarães, P. M. (2008). Combined free and forced coonvection in an inclined channel with discrete heat sources, Int. Communications of Heat and Mass Transfer, Vol. 35, pp. 1267-1274.

Convection and Conduction Heat Transfer

Edited by Dr. Amimul Ahsan

ISBN 978-953-307-582-2

Hard cover, 394 pages

Publisher InTech

Published online 17, October, 2011

Published in print edition October, 2011

The convection and conduction heat transfer, thermal conductivity, and phase transformations are significant issues in a design of wide range of industrial processes and devices. This book includes 18 advanced and revised contributions, and it covers mainly (1) heat convection, (2) heat conduction, and (3) heat transfer analysis. The first section introduces mixed convection studies on inclined channels, double diffusive coupling, and on lid driven trapezoidal cavity, forced natural convection through a roof, convection on non-isothermal jet oscillations, unsteady pulsed flow, and hydromagnetic flow with thermal radiation. The second section covers heat conduction in capillary porous bodies and in structures made of functionally graded materials, integral transforms for heat conduction problems, non-linear radiative-conductive heat transfer, thermal conductivity of gas diffusion layers and multi-component natural systems, thermal behavior of the ink, primer and paint, heating in biothermal systems, and RBF finite difference approach in heat conduction. The third section includes heat transfer analysis of reinforced concrete beam, modeling of heat transfer and phase transformations, boundary conditions-surface heat flux and temperature, simulation of phase change materials, and finite element methods of factorial design. The advanced idea and information described here will be fruitful for the readers to find a sustainable solution in an industrialized society.

How to reference

In order to correctly reference this scholarly work, feel free to copy and paste the following:

Paulo M. Guimarães and Genésio J. Menon (2011). A Mixed Convection Study in Inclined Channels with Discrete Heat Sources, Convection and Conduction Heat Transfer, Dr. Amimul Ahsan (Ed.), ISBN: 978-953-307-582-2, InTech, Available from: http://www.intechopen.com/books/convection-and-conduction-heat-transfer/a-mixed-convection-study-in-inclined-channels-with-discrete-heat-sources

INTECH
open science | open minds

InTech Europe
University Campus STeP Ri
Slavka Krautzeka 83/A
51000 Rijeka, Croatia
Phone: +385 (51) 770 447
Fax: +385 (51) 686 166
www.intechopen.com

InTech China
Unit 405, Office Block, Hotel Equatorial Shanghai
No.65, Yan An Road (West), Shanghai, 200040, China
中国上海市延安西路65号上海国际贵都大饭店办公楼405单元
Phone: +86-21-62489820
Fax: +86-21-62489821